MIT JOINT PROGRAM
SCIENCE POLICY
GLOBAL CHANGE

Report 357
February 2022

The Changing Nature of Climate-Related Risks in Global Wind Power Resources

C. Adam Schlosser, Sara Uzquiano Perez, and Andrei Sokolov

MIT Joint Program on the Science and Policy of Global Change combines cutting-edge scientific research with independent policy analysis to provide a solid foundation for the public and private decisions needed to mitigate and adapt to unavoidable global environmental changes. Being data-driven, the Joint Program uses extensive Earth system and economic data and models to produce quantitative analysis and predictions of the risks of climate change and the challenges of limiting human influence on the environment—essential knowledge for the international dialogue toward a global response to climate change.

To this end, the Joint Program brings together an interdisciplinary group from two established MIT research centers: the **Center for Global Change Science (CGCS)** and the **Center for Energy and Environmental Policy Research (CEEPR)**. These two centers—along with collaborators from the Marine Biology Laboratory (MBL) at Woods Hole and short- and long-term visitors—provide the united vision needed to solve global challenges.

At the heart of much of the program's work lies MIT's Integrated Global System Model. Through this integrated model, the program seeks to discover new interactions among natural and human climate system components; objectively assess uncertainty in economic and climate projections; critically and quantitatively analyze environmental management and policy proposals; understand complex connections among the many forces that will shape our future; and improve methods to model, monitor and verify greenhouse gas emissions and climatic impacts.

This report is intended to communicate research results and improve public understanding of global environment and energy challenges, thereby contributing to informed debate about climate change and the economic and social implications of policy alternatives.

—Ronald G. Prinn,
Joint Program Director

MIT Joint Program on the Science and Policy of Global Change

Massachusetts Institute of Technology
77 Massachusetts Ave., E19-411
Cambridge MA 02139-4307 (USA)

T (617) 253-7492 **F** (617) 253-9845
globalchange@mit.edu
http://globalchange.mit.edu/

GLOBAL CHANGE

FEBRUARY 2022

The Changing Nature of Climate-Related Risks in Global Wind Power Resources

C. Adam Schlosser, Sara Uzquiano Perez, and Andrei Sokolov

Abstract: Under the ambitious low-carbon goals set forth by the recent Paris Accord as well as the prospects for large penetration of renewable energy-generation technologies, the need for advances in quantitative insights and foresights into the current and future availability of renewable energy resources is greater than ever. We have analyzed the changing risks in worldwide wind-power resource availability using large-ensemble simulations that span a range of human-forced climate scenarios. To enable this analysis, we construct estimates of wind power density (WPD) via a hybrid method that combines the emerging patterns of change in near-surface winds from climate models with the large-ensemble, probabilistic projections of the MIT Integrated Global System Model (IGSM). Globally speaking, at a "75% consensus" threshold criterion (at least 3 out of every 4 members agree in the sign of change), by mid-century under an emissions scenario that assumes no further actions to limit emissions, an increase of about 2% in annual-averaged WPD is expected. Under the most aggressive mitigation scenario considered associated with a global climate warming target of 1.5˚C, the expected increase is reduced to 0.5%. There is a notable seasonality to these expected global changes, with global WPD increases during December-February, and decreases across all remaining seasons. Salient and coherent geographic patterns are also found, however, there is a strong sensitivity of these results to the strictness of model-trend consensus applied, particularly in the spatial extent of the results that exceed the consensus criterion. At 90% consensus (at least 9 out of every 10 ensemble members must agree in sign of change) only 5%-8% of globe passes this threshold in the ensemble of WPD changes. When contrasting the global-scale trends with respect to onshore and offshore regions, annual WPD will increase slightly offshore (median and average less than 1%) but slightly decrease onshore (-1% in the median), yet the seasonality of these WPD changes is more pronounced.

1. Introduction

To meet the increasing global importance and deployment of low-carbon technologies and energy generation, the need for advances in quantitative insights and foresights into the current and future availability of renewable energy resources (e.g. wind and solar) is greater than ever. The research community, industry, and government stakeholders share a common interest and goal for an enhanced understanding of renewable resources around the globe. Under the ambitious low-carbon goals set forth by the recent Paris Accord as well as the prospects for large penetration of renewable energy-generation technologies, this project's overall aim is to conduct and support analyses of the current and future availability in wind power resources. Any such mix and landscape of energy-generation will place a high premium on the predictability of directly relevant environmental conditions, and in doing so will support improved predictions in any shifts, oscillations, events, and trends of wind power in space and time—which are all determined by weather and climate.

One area of concern under the current global warming scenario regards the extent to which these associated weather and climate patterns might change in response to human interference of the climate system, whether climate mitigation may reduce any threat and if adaptive measures are warranted. Recent assessments (e.g. Karnauskas *et al.*, 2017) of climate models from the IPCC 5th Assessment report indicate that there are broad areas of the globe that indicate a consensus in annual changes of wind power associated with human-forced climate change, especially under stronger forcing scenarios and toward the end of the century. Other studies have fitted distributions of wind speed (e.g. Jung and Schindler, 2019) to assess the potential for change under future climate conditions, provided regional lenses to assess the historical conditions (e.g. Liu *et al.*, 2020, Enevoldsen *et al.* 2019, and Zeng *et al.*, 2019), evaluated climate model simulations (e.g. Tian *et al.*, 2019), as well as potential landscapes of wind power deployment under physical and technical constraints (e.g. de Castro *et al.*, 2011) and future low-carbon energy scenarios (e.g. Luderer *et al.*, 2017). Insights from these studies have lacked details in the seasonality and regional aspects. However, separate studies have focused on the impact of seasonally varying atmospheric conditions (e.g. Ulazai *et al.*, 2019), long term historical trends (e.g. Jung *et al.*, 2019) and the potential future changes of wind and/or wind power resource under a range of climate scenarios (e.g. Karnauskas, 2017). The use of regional climate models, with their enhanced spatial and process-level detail, have been used to look at the geographic details into potential future changes across regions and/or nations of interest (e.g. Gao *et al.*, 2019). Yet given the computational expense, such studies fall well short of a rigorous sample in the structural uncertainty in the models' response to potential regional climate change under a full range of plausible global scenarios. Therefore, despite all these recent advances and studies, quantitative knowledge of climate-related impacts on global and regional wind-power production remains adolescent. In view of these recent efforts—we have undertaken a study that considers seasonality supported by a large-ensemble, risk-based framework—and done so under timely and policy-relevant global commitments (i.e. COP21) and global targets (i.e. limit global warming to 2°C and 1.5°C by the end of century).

Broadly speaking, the overall scope is to conduct analyses that support and advance the current assessments on wind and solar power availability, (co-)variability, and (co-)intermittency using a variety of methods on multi-decade reanalyses as well as historical and experimental simulations of the future climate with state-of-the-art general circulation models. The analyses is global in scope but provides regional lenses across the globe where interests merit. As such, these simulations and corresponding analyses aims to:

- Assess the extent to which human-induced climate change will alter these patterns of wind and solar availability and variability. Holistically, the research will provide risk-based, quantitative insights to support large-deployment strategies for ambitious and transformational low-carbon energy goals—while also recognizing avoided as well as unavoidable climate changes that could substantially alter the landscape of renewable energy resources.
- Evaluate mean, variance, availability, and intermittency of (CMIP) models' estimates against reanalyses.
- Evaluate climate models' ability to reproduce the observationally-based extent, variability, intermittency, and extremes in wind and solar power production—particularly in association with large-scale weather patterns and climate oscillations.
- Analyze trends in the intermittency, variability and extremes of renewable energy production and their link to large-scale weather patterns and climate oscillations. Thereby providing a basis for their potential predictability.
- Derive a catalogue of synoptic patterns shaping energy production, defining connections between synoptic and meso/local scales.

The research is to be conducted in a successive fashion with respect to the topics listed above. In this first project stage and submitted in this report, we focus on an ability identify and assess locations with the highest risk to human-forced change. Therefore, the approach has been one of a "triage risk" approach. This assessment has been based upon methods developed in previous studies but updated with the more recent global scenarios and expanded in geographic scope and distributional detail. The analyses consider the benefits of the most recent COP21 commit-

ments as well as the more aggressive 2°C and 1.5°C global climate targets, and in doing provides an assessment of the extent to which changes are "unavoidable" (even under the most aggressive mitigation scenarios) and adaptive (or proactive) measures and decisions to future deployment should be considered. As these regions are identified, it is anticipated that subsequent (and/or additional) analyses could be performed to provide more specific and detailed tools and models to evaluate and quantify the causes and extent of human-forced predictability and risk across intra-seasonal to decadal timescales—and associate these with and against large-scale climate oscillations and trends.

2. Research Methods

The overall framework of this assessment is "triage based", and in doing so, it aims to provide a purview of regional risks to wind power density (WPD) changes. These analyses focuses on the impact of climate mitigation efforts to the risk of change, indicates the extent of unavoidable human-induced climate-related change, and can identify hotspots of change and regions in need of deeper inspection and analyses. Overall, our analysis is governed by acquiring information from global scale data on the historical and future near-surface atmosphere conditions that allow us to estimate WPD as:

$$Wind\ Power\ Density\ (WPD_z) = \tfrac{1}{2}\rho_z V_z^3 \quad (1)$$

For any given hub height (z) under consideration, we use information on air density (ρ_z) and windspeed (V_z). In this assessment, we present results for a 100 m hub height (z=100 m), which is the typical hub height for current large, multi-megawatt wind turbines. While we have performed these calculations at other hub heights for other studies to assess the advantage of higher turbines on intermittency and mean resource (e.g. Gunturu and Schlosser, 2012; Cosseron *et al.*, 2014), this is outside the scope of the current phase of this project. For brevity, the z subscript will be dropped from all these terms hereafter and any reference to these terms will be related to the 100m height unless otherwise stated explicitly. The research approach creates historical estimates of the WPD resource (e.g. **Figs. 1 and 2**), using supporting historical data (described below). Then using information from modeled climate changes, we apply geographical changes to the historical estimates that are scaled according to "pattern change kernels" that describe the (relative) local sensitivity of windspeed to the global forcing (and warming) of climate. These geographical changes to WPD are provided in a risk-based context, whereby large ensembles of projections (1,000s of simulations) are generated against a prescribed scenario of a socio-economic and/or climate-target policy of the future. Under this construct, these large ensembles provide a distribution of outcomes for a given aspect of the environment that is of interest—in this case WPD.

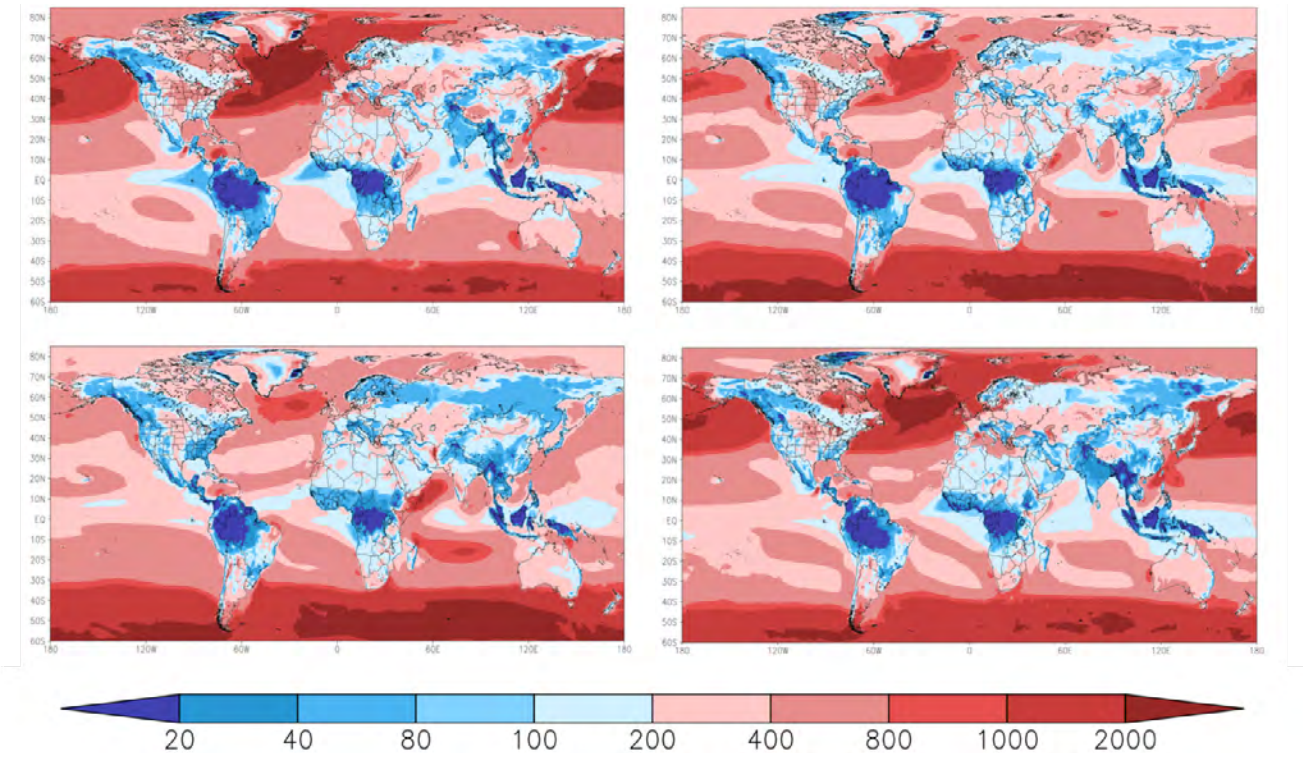

Figure 1. Seasonally-averaged maps of wind power density (WPD, units of W/m^2) for: a) December-February; b) March-May; c) June-August; and d) September-November. Results are based on data from the Modern-Era Reanalysis for Research and Applications Phase 2 (MERRA2). See text for details. The seasonal averages are based on MERRA2 data for the years 2010-2019.

While this model construction allows for a continuous timeseries of future trajectories (e.g. **Figs. 3 and 4**), we will focus our attention on the decadal-averaged changes in WPD that occur by mid-century. In the sections that follow, we describe the supporting data, models, and methods employed.

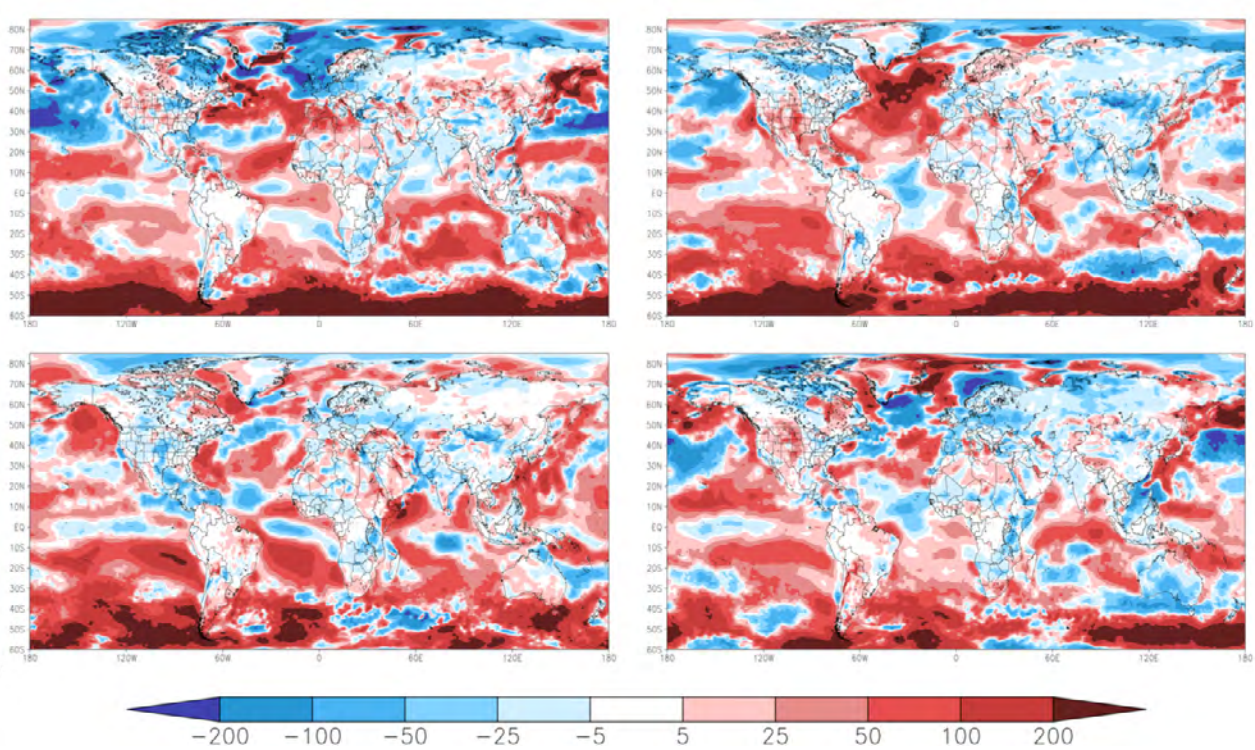

Figure 2. Seasonally-averaged maps of changes in decadal mean wind power density (WPD, units of W/m^2) for the 2010-2019 from the 1980-1989 period. Maps display results for a) December-February; b) March-May; c) June-August; and d) September-November. Results are based on data from the Modern-Era Reanalysis for Research and Applications Phase 2 (MERRA2). See text for details.

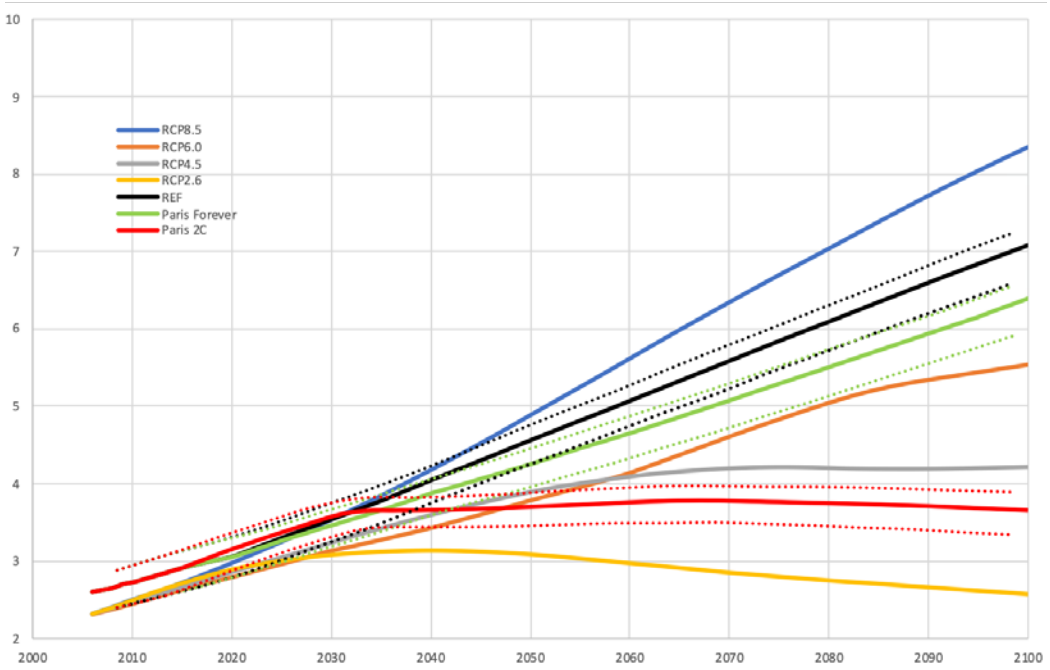

Figure 3. Comparison of the total radiative forcing (relative to 1860) from a selection of the MIT IGSM scenarios used in this study, compared to the simulations from the Representative Concentration Pathway (RCP) experiments. Units are in W/m^2.

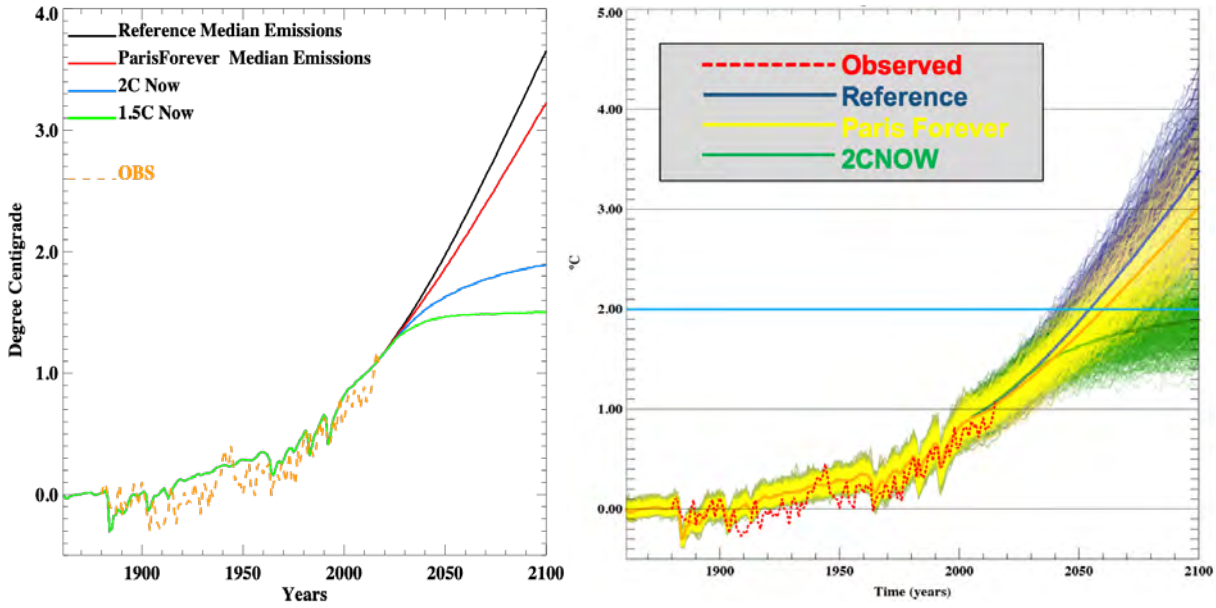

Figure 4. Global averaged annual surface-air temperature trends as simulated by the MIT IGSM. The left panel presents the median trajectories of the IGSM ensemble. The right panel provides the trajectories from all ensemble members for a selection of the scenarios performed by the IGSM. Trends in temperature are calculated relative to the 1861-1880 mean.

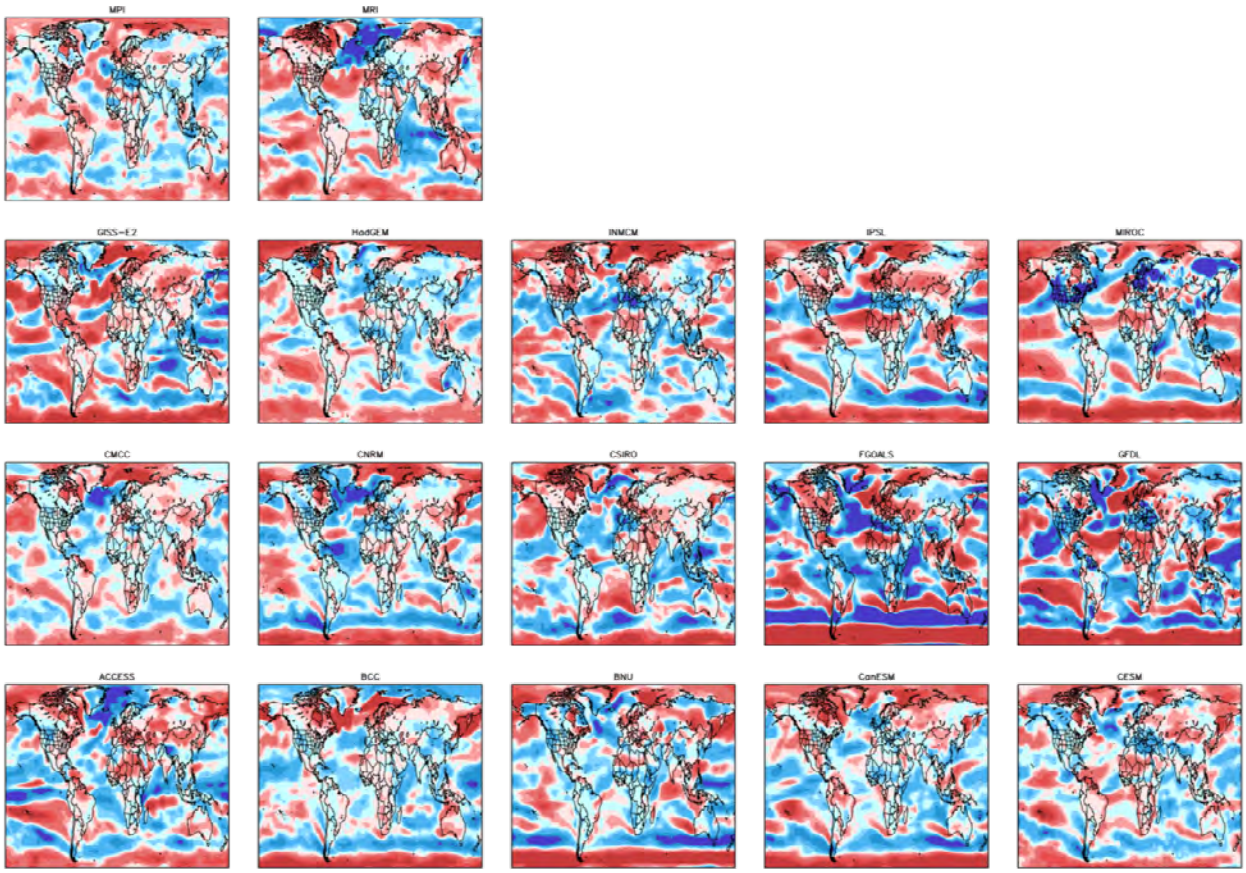

Figure 5. Pattern-change kernels (PCKs) that describe the relative change in near-surface windspeed (to its global value) per unit change in global averaged surface-air temperature (units of K^{-1}). Maps show the PCKs derived from each of the participating models in the Coupled Model Intercomparison Project Phase 5 (CMIP5). PCKs are derived for each month from the 1% transient CO_2 experimental simulations. These maps display the December-February averaged results.

2.1 Supporting Historical Data

Reanalysis data are interpolations of discontinuous (in space and time) observational data based on a dynamical model and are therefore complete, physically consistent, multi-decade data sets of environmental states and fluxes. We have used for our baseline assessment of WPD, an estimate based on the Modern Era Retrospective-analysis for Research and Applications Version 2 (MERRA2, Reinecker *et al.*, 2011). The choice of MERRA2 is based upon prior studies and analyses of WPD conducted with the MERRA data products (e.g., Gunturu and Schlosser, 2015; Hallgren *et al.*, 2014; Fant *et al.*, 2016; Kriesche and Schlosser, 2014; Cosseron *et al.*, 2013). The MERRA2 uses the GEOS-5 atmospheric circulation model, the Catchment land surface model, and an enhanced three-dimensional variational data assimilation (3DVAR) analysis algorithm. The data assimilation system of GEOS-5 implements Incremental Analysis Updates (IAU) procedure in which the analysis correction is applied to the forecast model states gradually. MERRA's physical parameterizations have also been enhanced so that the shock of adjusting the model system to the assimilated data is reduced. In addition, MERRA incorporates observations from NASA's Earth Observing Systems (EOS) satellites, particularly those from EOS/Aqua, in its assimilation framework. The MERRA is updated in real time, spanning the period from 1979 to the present. The three-dimensional 3 hourly atmospheric diagnostics on 42 pressure levels are available at a 0.5° latitude by 0.6° longitude grid resolution. This uses near-surface conditions of: surface pressure (at 2-meter height), near-surface wind speed, air temperature (at 2 meter height) in order to make the estimates of WPD. Torralba *et al.* (2017) evaluated three sources of reanalysis data provided by various institutes, MERRA2 among them (ERA and JRA the other two), and found consistencies in the large-scale changes (i.e. ocean vs. land) across their multi-decade timespan (1980-2015). An example of these seasonally-averaged large scale current conditions and changes are shown in Figures 1 and 2 (showing the decadal averages and changes in WPD between the 1980s and 2010s).

2.2 Model Scenarios

As mentioned, projections of WPD change are based upon a hybrid approach that combines rigorous, large-ensemble human-Earth system simulations to provide a comprehensive range of the global climate response with a range of patterns in the response of windspeed that are associated with global, human-forced climate warming. The models used in this hybrid approach developed are described below. We are only using the decadal mean values of estimated WPD as a baseline such that the projections of potential changes in WPD are added to it.

The set of scenarios from the human-Earth system framework for this exercise was selected from the 2018 Food, Energy, Water, and Climate Outlook produced by the MIT Joint Program on the Science and Policy of Global Change (Reilly *et al.*, 2018). The scenarios, each run under a large ensemble of 400 members, are constructed with the MIT Integrated Global System Model (IGSM) that includes the MIT Earth System Model (MESM, Sokolov *et al.*, 2018). The IGSM-MESM is able to consider a broad range of uncertainties Earth systems' behavior and response to natural and anthropogenic drivers (e.g. Libardoni *et al.*, 2018), and also span a range of global emissions policies and are based on a regionally detailed, multi-sector, economy-wide model that includes pricing of fossil fuels, fossil resources, and vintage capital in capital intensive sectors (e.g. Chen *et al.*, 2016). Under the policy scenarios, prematurely retired capital stock and the need to replace conventional energy sources with more expensive, low-carbon options draw investment resources away from other sectors of the economy and, thus, have an impact on GDP growth in mitigation scenarios. The reduced GDP thereby reduces investment overall in the mitigation scenarios. However, it is reallocated toward those energy sources that meet the emissions reduction targets at least cost.

Four scenarios, developed to span a range of possible global actions to abate greenhouse gas emissions over the coming century, were used to explore climate-change risks.

Reference (REF): This scenario has no explicit climate mitigation policies anywhere in the world. Thus, it represents a world in which there is no Paris Agreement and no alternative action towards reducing emissions for the sake of limiting climate change. However, it includes some energy policies such as fuel economy standards, renewable electricity requirements, and the gradual phase-out of old coal power plants that are presently occurring with various motivations. These motivations include reducing imported oil dependence, using less of exhaustible resources, or to reducing conventional pollutants. Such efforts may in part reflect concerns about climate change, but the policies have no specific greenhouse gas emissions targets. The REF serves as a baseline scenario because of its simplicity. Metrics from the other scenarios are often presented as the difference between another scenario and the REF scenario. It provides the upper assessment of our modeled physical risks.

Paris Forever (PF): Countries meet the mitigation targets in their Nationally Determined Contributions (NDCs) and continue to abide by them through the end of the century. The Paris Agreement includes NDCs submitted at the 2015 Paris Conference of the Parties (COP) of the Framework Convention on Climate Change (FCCC). These NDCs—aimed at the reduction of CO_2 and other GHG emissions—generally deepened and extended through 2030 those made at the 2009 Copenhagen COP through 2020. These reductions are typically expressed as (1) an absolute emissions target (ABS), measured as an annual

level of emissions measured in Mt, (2) a percentage reduction from a pre-determined baseline, which can easily be converted into an absolute emissions target, or (3) an emissions intensity target (INT), measured as emissions in relation to GDP.

2CNOW: This scenario aims to limit climate warming to no higher than a 2°C global average at 2100. This is achieved by implementing a globally coordinated, smoothly rising carbon price—such that emissions are reduced. Variations in mitigation policies result in the overall uncertainty of different patterns of resource and energy use, different choices of technology, and drag on overall economic growth. This is also combined with the uncertainty of the global climate response that is represented in the MIT Earth System Model (MESM, Sokolov *et al.*, 2019). As described in Reilly *et al.* (2018)—these co-evolving uncertainties projected within a Latin-hypercube sampling results in an overall probability of achieving the target at 66%.

15CNOW: Similar to the 2C, this scenario aims to limit climate warming to no higher than 1.5°C global average at 2100. Under the similar Latin-hypercube sampling of structural uncertainties within the Earth and human model systems, this results in a 50% probability of achieving the climate target (i.e. 200 of the 400-member ensemble meets the target).

These scenarios result in distinct pathways and distributions of global averaged changes in human forcing and climate variables (Figs. 3 and 4). The mid-century impact of the more aggressive climate-based targets (i.e., 15CNOW and 2CNOW scenarios) is distinguished by the majority of their distribution of outcomes falling outside the distribution of the REF scenario. In addition, shifts in the modal value of change, the percentage of the distribution at the modal value, as well as the total range of outcomes (i.e. width of the distribution) highlight the notable impact of the aggressive climate targets at reducing (and eliminating) the risk of strongest changes. The PF scenario, which captures the current global commitments to reduce emissions (under the Paris Agreement), shows a discernible shift toward lower risks of change, yet considerable overlap (particularly for surface-air temperature) with the REF distributions remains by mid-century. Given all these considerations, we can then gauge the extent of how these global results translate into regional features of risk through a procedure described in the next section.

2.3 Regional Climate-Change Pattern Kernels

The aforementioned scenarios are conducted with the MIT Integrated Global Systems Model (IGSM) framework. The underlying motivation for the approach exercised in this research is driven by the MIT Earth Systems Model (MESM, Sokolov *et al.*, 2018) providing probabilistic projections of atmospheric conditions at the zonal level of detail. In order to provide regional texture to the MESM simulations, we must expand this information across longitudes using a "pattern scaling" method tailored to the MESM configuration. The use of pattern-scaling methods in climate-change scenario assessments and impact studies is extensive and varied (e.g., Santer *et al.*, 1990; Wigley *et al,* 2000; Mitchell, 2003; Frieler *et al.*, 2012; Lopez *et al.*, 2013; and Herger *et al.*, 2015). For our particular application to the MESM framework, the full description and evaluation of the methodology is provided in Schlosser *et al.* (2012), and herein we describe the key features of this transformation procedure as applied to this wind power assessment. In the simplest terms, for any MESM-simulated zonal variable of interest, V_y, at a given latitude (y) under a human-forced global temperature change (ΔT_G), we can write a transformation of that variable's value at a given longitude (*x)* along the latitude band using the following Taylor-expansion based numerical relationship:

$$V_{x,y}(\Delta T_G) = \overline{C}_{x,y} V_y + \left[\frac{dC_{x,y}}{dT_G}\Delta T_G\right] V_y \qquad (2)$$

where $\overline{C}_{x,y}$ is the climatological downscaling transformation coefficient (altering the zonal mean value to assign a particular value for a longitudinal point along the zonal band) for any reference time period, and we base this climatological coefficient on the observational data record (described in section 2.1). The projected change in globally averaged temperature, ΔT_{Global}, is relative to a reference or climatological period (1980-1999). The derivative of these transformation coefficients, $\frac{dC_{x,y}}{dT_G}$, for any point (x,y) are discretely estimated from climate model information (for further details, see Schlosser *et al.*, 2012, Section 2 methodology discussion of Equation 4). Therefore, we consider and hereafter refer to the $\frac{dC_{x,y}}{dT_G}$ terms as "pattern-change kernels" (PCKs), and these PCKs describe the shifts to $\overline{C}_{x,y}$ associated with human-forced climate warming. We construct a set of these PCKs from a selection of the CMIP5 climate models (**Table 1**), and as a result, this provides the regional details to the large ensembles constructed by IGSM MESM (discussed in Section 2.2). These simulations were all conducted in a consistent fashion across the participating climate models, and were designed to explore the sensitivity of their simulated climates against the human-forced increase in (equivalent) radiatively active trace-gas concentrations (a.k.a. "greenhouse" gases). As a result, this procedure provides the regional basis for the large ensemble of response patterns and allow us to construct distributions of change. The CMIP5 model archive provides a comprehensive set of outputs from climate and Earth-system models that have been developed at institutes across the international scientific community. In some cases, these institutes submitted multiple results that were conducted by

Table 1. List of CMIP5 models used to construct the pattern-scaling kernels of climate change response. Shown are the model acronyms, institute/model name, and the horizontal spatial resolution of the model's output used.

Model Acronym	Model/Institute	Resolution
ACCESS1-3	Australian Community Climate and Earth-System Simulator	1.875° x 1.25°
BCC-CSM1-1-m	Beijing Climate Center	1.125 ° x 1.125°
BNU-ESM1	Beijing Normal University	2.8125° x 2.8125°
CanESM2	Canadian Earth-System Model	2.8125° x 2.8125°
CESM1-BGC	Community Earth System Model (NCAR)	1.25° x 0.9375°
CMCC-CM	Centro Euro-Mediterraneo Cambiamenti Climatici Climate Model	0.75° x 0.75°
CNRM-CM5	Centre National de Recherches Meteorologiques	1.40625° x 1.45°
CSIRO-Mk3-6-0	Commonwealth Scientific and Industrial Research Organization	1.875° x 1.875°
FGOALS-s2	Flexible Global Ocean-Atmosphere-Land System	2.8125° x 1.66°
GFDL-CM3	Geophysical Fluid Dynamics Laboratory	2.5° x 2.0°
GISS-E2-R	Goddard Institute for Space Studies	2.5° x 2.0°
HadGEM2-ES	Hadley Centre Global Environmental Model	1.875° x 1.25°
INMCM4	Institute of Numerical Mathematics	2.0° x 1.5°
IPSL-CM5B-LR	L'institut Pierre-Simon Laplace Coupled Model	3.75° x 1.875°
MIROC5	Model for Interdisciplinary Research on Climate	1.40625° x 1.40625°
MPI-ESM-MR	Max Planck Institute	2.5 x 1.25°
MRI-CGCM3	Meteorological Research Institute	1.125 x 1.125°
NorESM1-M	Norwegian Earth System Model	2.5 x 1.875°

their model under a variety of different configurations (e.g. different spatial resolutions and/or various parameterization prescriptions). In constructing this meta-ensemble, we did not incorporate "sibling" model results and instead selected only one set of model results per institute to determine a representative PCK. This was done in order to avoid biasing in the meta-distribution that would result from using "sibling" PCKs (and thereby inappropriately stacking a particular regional response pattern of change). Given the problematic nature of assessing the relative fidelity climate model projections (e.g. Reifen and Toumi, 2009), there was no preferential selection to one model result (e.g. the highest spatial resolution) when multiple configurations were available from an institute. This was also done so as to avoid any other possible sources of biasing when deriving these PCKs across all the models/institutes, and to achieve a diverse sampling of outcomes across the range of climate model structures. As a result, the model results from 17 distinct institutes that participated in the CMIP5 exercise were used. (**Table 1**). Each of the PCKs were constructed at the native model resolution, and then interpolated to a 2°x2.5° (approximately 200 km x 250 km) common grid (shown in **Figs. 6-10**), which was commensurate with the coarsest model grid from the CMIP5 model pool.

With the constructed PCKs, we combine them with the 400 members of a MESM model scenario via the analytical relationship of (2) to obtain patterns of change for a meta-ensemble of 6,800 members per scenario. This 6,800-member meta-ensemble we refer to as a "hybrid frequency distribution" (HFD), and it is this set of results that is used as the basis of our risk quantification, and the impact of global policy and climate targets, in the regional analysis. Each HFD is used as the basis of our risk quantification and represents the range of outcomes that results from the global and regional structural uncertainties (from MESM and the PCKs).

An additional consideration in the construction of these windspeed pattern projections to the historical WPD assessment of the MERRA2 fields (i.e. Fig. 1), the near-surface wind field from the CMIP5 models must be scaled accordingly to the consistent hub height applied the MERRA2 assessment (100m). To do this, we apply a wind profile power law as used in a number of recent studies to extrapolate near-surface wind speed (at 10m height) to a desired hub height (e.g. Karnauskas *et al.*, 2017, Lee *et al.*, 2018; Ulazia *et al.*, 2019; Tian *et al.*, 2019; and Zeng *et al.*, 2019), which for this study has been chosen at 100m. As a precursory assessment, we summarize the model-mean, consensus and diversity of the PFKs across the CMIP5 models as well as the corresponding results from the MESM simulations.

Overall, the PCKs exhibit a rich variety in the pattern response of windspeed due to trace-gas forced climate warming (**Figs. 5-7**). However, when looking at the model-mean PCK response (**Fig. 8**), there are large-scale structures that are persistent across the entire year (i.e. seen in all the seasonally-averaged results) as well as seasonally distinct features. Specifically, there is an overall tendency that the

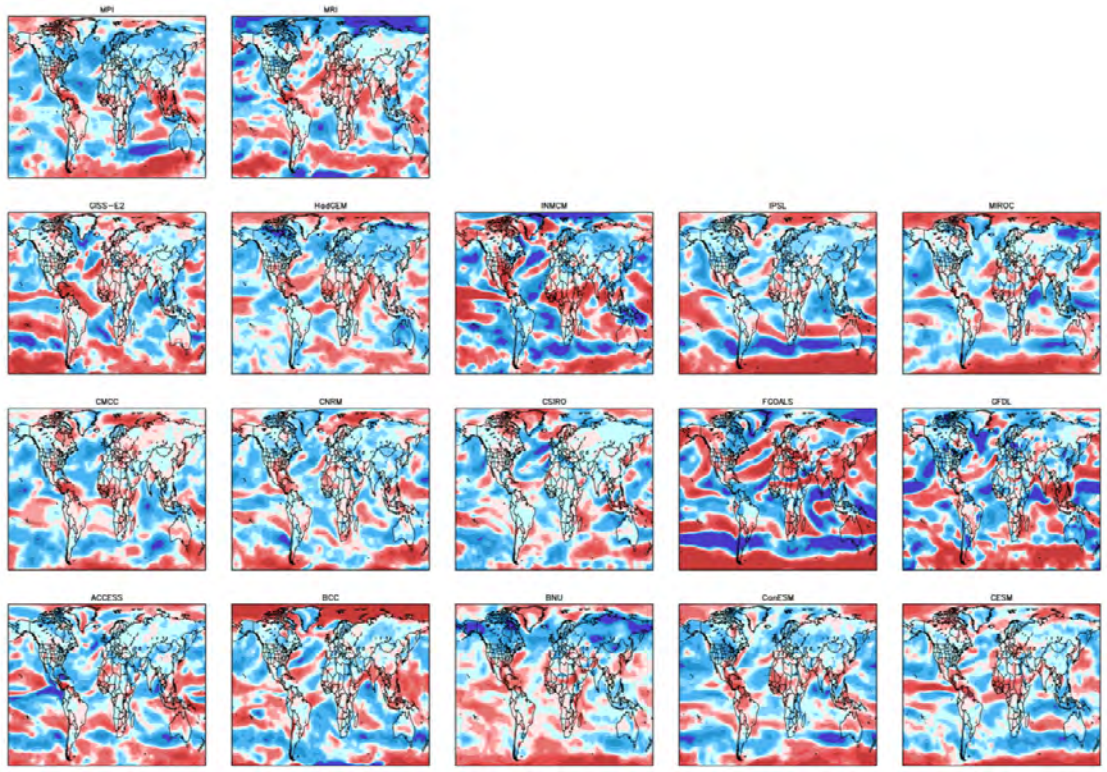

Figure 6. Pattern-change kernels (PCKs) that describe the relative change in near-surface windspeed (to its global value) per unit change in global averaged surface-air temperature (units of K^{-1}).

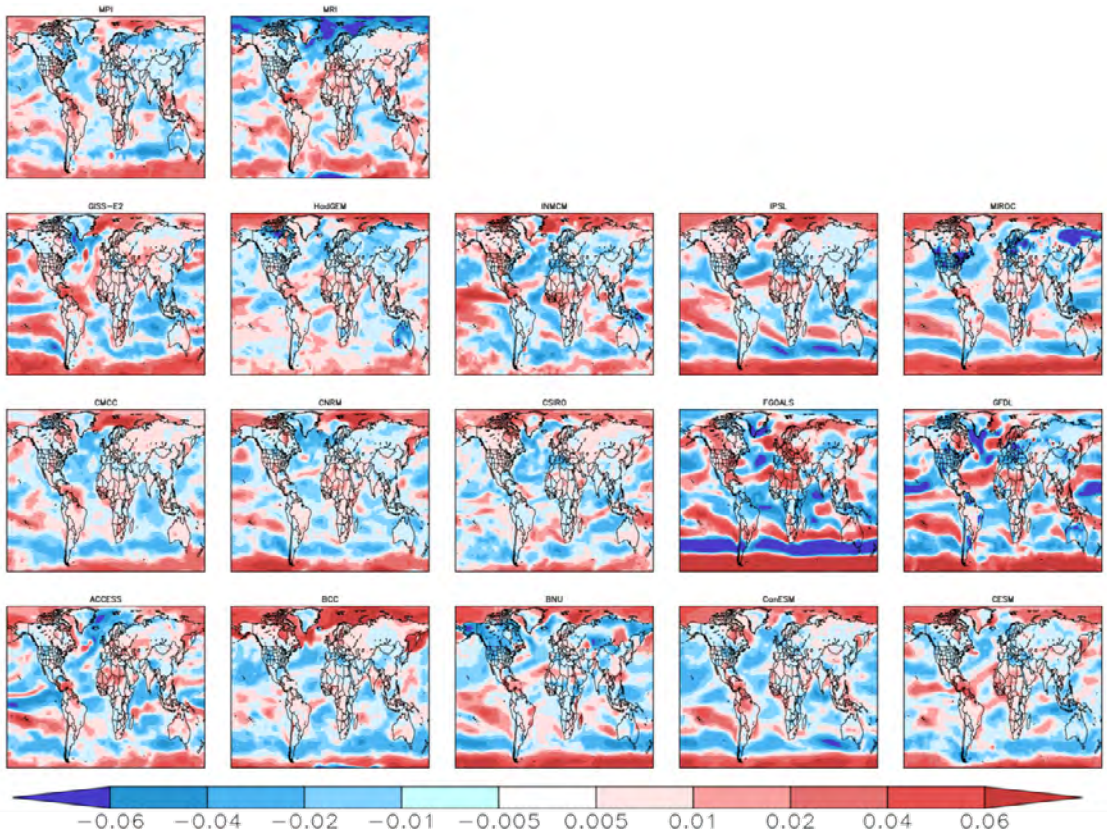

Figure 7. Pattern-change kernels (PCKs) that describe the relative change in near-surface windspeed (to its global value) per unit change in global averaged surface-air temperature (units of K^{-1}).

Maps show the PCKs derived from each of the participating models in the Coupled Model Intercomparison Project Phase 5 (CMIP5). PCKs are derived for each month from the 1% transient CO_2 experimental simulations. These maps display the annually averaged results of the monthly PCKs.

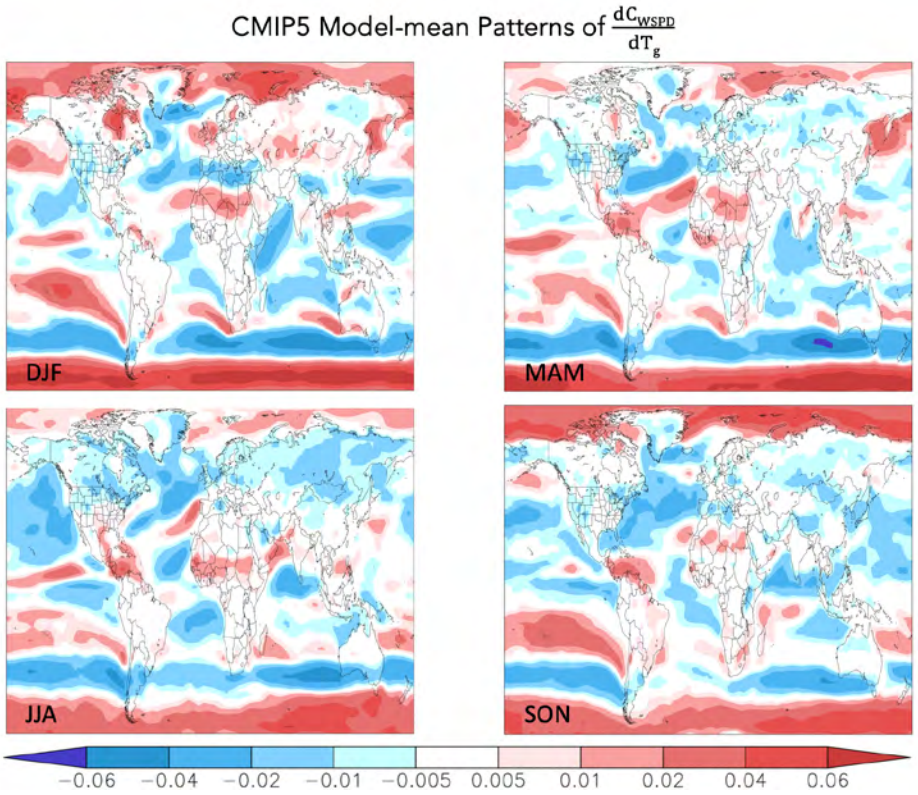

Figure 8. Pattern-change kernels (PCKs), , that describe the relative change in near-surface windspeed (to its global value) per unit change in global averaged surface-air temperature (units of K^{-1}). Maps show the CMIP5 model-mean PCKs. Shown are the seasonally averaged results for: Dec-Jan, DJF (upper left), Marc—May MAM (upper right), June-Aug, JJA (lower left), and Sept-Nov, SON (lower right).

magnitude of change in windspeed (whether up or down with climate warming) is stronger over ocean regions than over land. In addition, there is a strong dipole pattern across the high latitude Southern Hemisphere—and less distinctly so in the Northern Hemisphere. These high-latitude dipole patterns are consistent with prior studies (e.g. Karnauskas *et al.*, 2017), and is likely a signature of a poleward progression of extratropical storm systems. Perhaps also associated with extratropical storm activity is a decreasing tendency of windspeed (with climate warming) across the North Atlantic—and coincident with extratropical storm tracks, during the northern hemisphere winter months this decreasing tendency extends into the Mediterranean. Among the more salient and widespread seasonal features to these PCKs is seen across northern hemisphere summertime land regions, showing a tendency for windspeeds to decrease with climate warming. On an annual basis (**Fig. 9**), these aforementioned features are still discernable—but to varying degrees. The most prominent features are the high latitude dipoles (strongest over ocean regions) across the southern hemisphere and a widespread decrease response across the North Atlantic. The decreasing tendency over northern hemisphere land regions is also seen.

3. Results

3.1 Features and impacts of model-response consensus

As mentioned, the focus of the presented analyses will be to assess changes in mean WPD across 10-year averaging windows. This averaging window has been indicated in recent studies (e.g. Lee *et al.*, 2018) to be a sufficient period to assess wind power resource metrics at monthly/seasonal/annual increments. Upon visual inspection of the PCKs (i.e. **Figs. 6-8**), it is apparent that the emerging response (or behavior) of windspeed as simulated by climate models carries a potentially wide range of values. Our initial interest was to provide a first-order assessment of the consensus in the model response patterns, or namely, the consistency in the sign of change in response to forced climate warming (via radiatively active trace gas concentrations). On an annual basis (Fig. 9, right panel), we find that the majority of the model consensus occurs over oceans, but with some notable areas over land regions in South America and Africa, and to a lesser extent North America and along the Mediterranean region of Europe. As a result, the extent of the regions (Table 1) for which the mean change in WPD represents the "majority" of the results is considerably reduced (particularly over land regions) when applying a modest spatial filter (**Fig. 11**). For example, consistent with

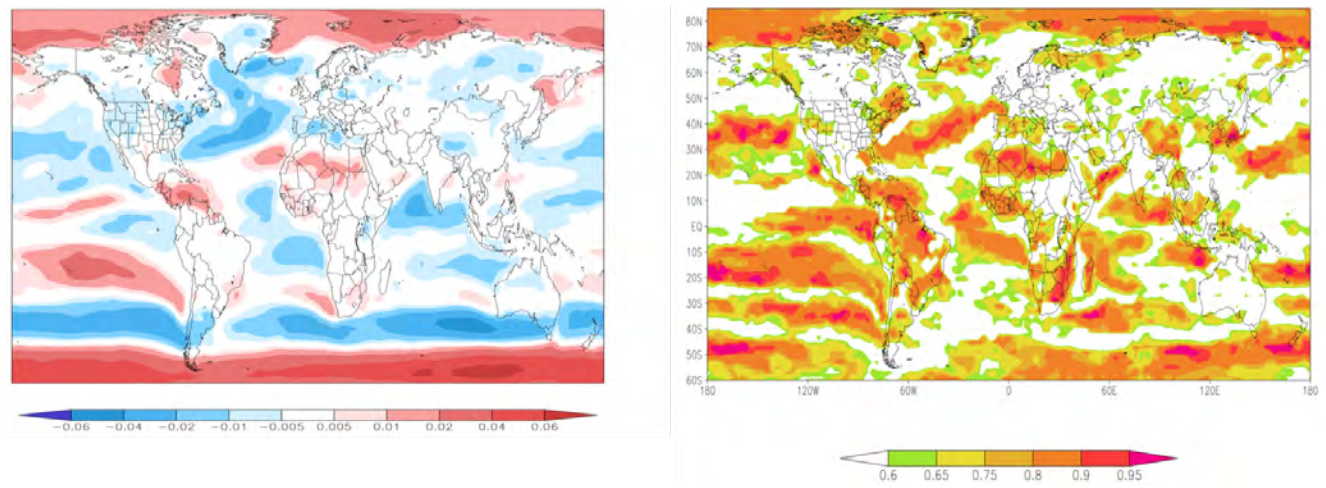

Figure 9. Maps depict the CMIP5 model mean (left panel) and consensus (right panel) in the estimated annual windspeed pattern-change kernel (PCKs, units in K^{-1}). For the left panel, the map displays the mean PCKs across all the CMIP5 model results (shown in Fig. 8). In the right panel, the map displays the fraction of the CMIP5 PCKs that agree with the sign of the model mean value (shown in the left panel).

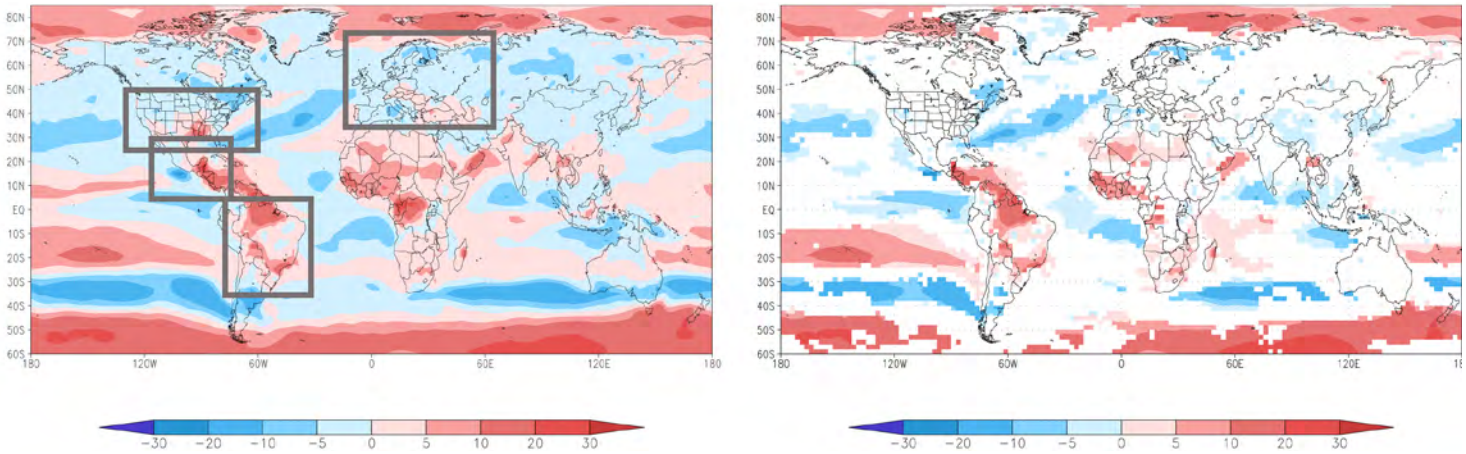

Figure 10. Global results of the change to annual wind power density (WPD) by midcentury as simulated in the IGSM Reference scenario. Results are shown for the relative change (%) of the decadal averaged mean WPD for the period 2050-2059 from the 2010-2019 period. Shaded values represent the mean result from the IGSM ensemble simulation. The left panel displays the results that have not been filtered, while the right panel display the results that have been filtered out if the models' consensus in the sign of the simulated trend does not exceed 75%. In addition, the gray outlined regions in the left panel denote the boundaries for area-averaged results presented in Tables 2-6.

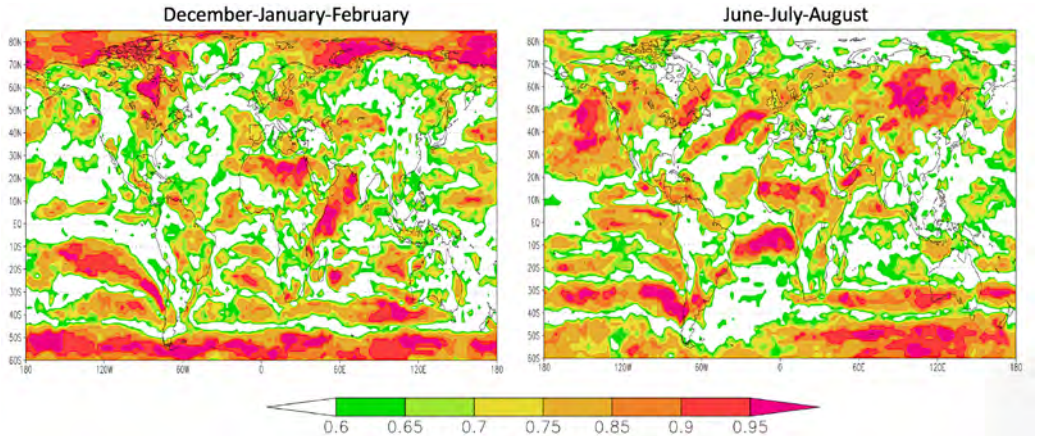

Figure 11. Maps show the consensus in CMIP5 pattern-change kernels (PCKs). In each panel, the fraction of the CMIP5 PCKs that agree with the sign of the model mean PCK (Fig. 8) is shown. Left panel displays the results for the seasonally averaged PCKs for December through February and the right panel for the June through August average.

the "more likely" nomenclature of the IPCC characterization of confidence, by applying a criterion of at least 75% of the model ensemble members (totaling 6,800) agree in the sign of the trend, we find that at a global scale, the fraction of the area that meets this condition is roughly 1/3 (or 33%) of the globe (**Table 2**, top five rows, middle column). Given this, globally speaking, for these regions of the globe where a 75% consensus is met, the annual, area-average WPD is 602 W/m^2 (with a small seasonality) and indicates that by mid-century under our REF scenario an ensemble-mean increase of about 2% (**Table 3**). This is, by no means, indicative of a spatially uniform response. The regions with the most notable deviation to the global change response are seen over North America and Europe (**Fig. 10**), showing decreases in WPD of -5% and -2.5%, respectively (Table 3). These decreases are a result of responses that persist across all but the NH winter seasons (**Tables 4-7**).

Overall, the impact of the consensus filtering is to intensify the (relative) change in area-averaged WPD (Tables 3-7). This effect is, perhaps, not surprising given that the relative maxima patterns of the PCKs and locations of the strongest model consensus largely coincide (Fig. 10, comparing left and right panels). Therefore, as the consensus threshold is increased, the impact of the higher sensitive areas of the PCKs is isolated (**Fig. 11**). In this context, the spatial coincidence of model consensus and PCKs is also seen across seasons, with a number of the aforementioned salient features in the model patterns accentuated as such (Figs. 8 and 11). During the northern hemisphere (NH) summer (June-August), much of coherent areas of decreasing windspeed over North America and Asia exhibit model consensus that exceeds 75%, while the extent of

Table 2. Summary of results for varying degrees of model-trend consensus filtering. In the rightmost column, the annual and seasonal means: Dec-Feb (DJF), Mar-May (MAM), Jun-Aug (JJA), and Sep-Nov (SON), area-averaged estimate of wind power density (WPD, units in W/m^2) is provided. The estimate is based on the MERRA2 values averaged for the 2010-2019 period (see Fig. 2). The middle columns depict: the percentage area for which the model consensus threshold is met, and embolden in parenthesis, the historical area-averaged WPD for the region (in W/m^2) is provided based on only those points that have met the consensus threshold.

Region		Percentage of Area Above Trend Consensus Threshold and (Area-Averaged WPD, in W/m^2, Above Threshold)			Unfiltered Area-Average WPD (W/m^2)
		60% Model-Trend Consensus	75% Model-Trend Consensus	90% Model-Trend Consensus	
Globe 180W-180E 60S-85N	Annual	57.3 (611)	36.0 (602)	5.0 (885)	567
	DJF	62.2 (617)	34.2 (702)	8.2 (917)	582
	MAM	57.3 (616)	26.6 (751)	4.2 (1217)	552
	JJA	64.2 (626)	38.1 (680)	7.8 (822)	572
	SON	66.3 (586)	39.0 (605)	5.1 (583)	561
Central America 113E-73E 15N-30N	Annual	55.0 (270)	37.8 (256)	0.1 (197)	245
	DJF	43.8 (322)	11.2 (220)	0.8 (242)	306
	MAM	56.3 (292)	32.0 (321)	4.7 (258)	258
	JJA	57.3 (209)	34.0 (187)	5.6 (92)	187
	SON	73.5 (258)	45.4 (296)	0.1 (N/A)	228
Brazil 75W-30W 35S-5N	Annual	67.1 (181)	45.5 (160)	6.3 (113)	202
	DJF	59.3 (151)	23.3 (127)	0.8 (19)	165
	MAM	54.9 (149)	22.9 (145)	2.8 (70)	166
	JJA	52.4 (223)	24.7 (226)	4.2 (268)	237
	SON	77.5 (202)	49.3 (142)	6.3 (95)	241
United States 130W-60W 25N-50N	Annual	49.8 (383)	29.2 (399)	0.7 (433)	273
	DJF	46.8 (503)	19.1 (490)	1.2 (410)	483
	MAM	57.4 (432)	31.7 (440)	2.9 (471)	395
	JJA	64.7 (217)	42.6 (205)	4.0 (120)	211
	SON	62.1 (381)	34.9 (461)	1.3 (732)	329
Europe 12W-65E 34N-75N	Annual	36.8 (330)	13.7 (316)	0.6 (511)	358
	DJF	70.7 (478)	31.8 (464)	3.4 (749)	497
	MAM	41.5 (323)	12.8 (264)	0.2 (300)	352
	JJA	68.1 (206)	39.2 (210)	2.5 (371)	215
	SON	42.2 (311)	16.4 (326)	1.0 (625)	368

this coincident behavior is reduced substantially during the NH winter (December-February). In a similar fashion over ocean regions, we find an extensive and strong area of consistency over the North Pacific and South Atlantic Oceans during the NH summer that is absent during the winter—and conversely exhibited across the Arctic Ocean, Southern Pacific Ocean, and over the Arabian Sea (i.e. strong consistency in NH winter). In all of these noted instances, the ensemble mean response is preserved for the 75% consensus criterion (**Figs. 12 and 13**). An additional salient feature over land at this level of consensus is the area of increased WPD across Africa—lying along the southern flank of the Sahel during the NH summer and then across the Saharan desert in NH winter. At the strongest level of a consensus threshold considered (90%, Figs. 12 and 13, lower right-hand panels), we find only two salient features of WPD change to remain over land regions: an increase in WPD across sub-tropical, northern Africa, and a decrease across eastern Asia. There are isolated decreases in WPD across the midlatitude South and North America that also remain—.

3.2 Impact of Mitigation and Unavoidable Risk

Given the aforementioned features surrounding model consensus, we focus our attention on the 75% consensus results to assess the impact of global emissions reduction and/or climate targets on the WPD mid-century changes (**Figs. 14 and 15**, **Tables 3-7**). Globally speaking, for the regions that exceed the 75% consensus criterion, the effect of strong mitigation actions (i.e. the 2CNOW and 15CNOW scenarios) is to halve the changes in WPD that would have occurred without those measures. However, it is worthy to note that the globally averaged response of WPD to human-forced climate warming is to increase the WPD potential, and among the regions of interest in this study, Brazil is likely to experience the strongest relative increases in WPD. This is in strong contrast to the relative decreases

Table 3. The summary presents the annual results of the relative change in wind power density (units of %). The relative changes reflect the decadal mean annual differences between midcentury (2050-2059) from the 2010-2019 average. As in Table 1, results are presented as area-averaged results for the globe as well as over selected regions: Central America (113W-73W,15N-30N), Brazil (75W-30W, 35S-5N), United States (130W-60W,25N-50N), and Europe (12W-65E,34N-75N). The area-averaged results are shown as a result of varying degrees of model-trend consensus spatial filtering—with grid points excluded from the area-average calculation if they do not exceed the assigned consensus threshold. Also shown are the unfiltered (UF) results.

Region	Scenario	**Area-Average Relative Change in Annual Wind Power Density (%)** Calculated Across a Range of Spatial Filters According to Modeled Trend Consensus			
		UF	**60%**	**75%**	**90%**
Globe	Reference	0.8	1.3	2.0	2.6
	Paris Forever	0.6	1.1	1.6	2.0
	2C-NOW	0.3	0.6	0.8	0.8
	1.5C-NOW	0.1	0.3	0.5	0.4
Central America	Reference	0.8	0.7	-0.3	-1.9
	Paris Forever	0.6	0.0	-0.4	-1.8
	2C-NOW	0.3	-0.3	-0.4	-1.5
	1.5C-NOW	0.1	-0.2	-0.4	-1.2
Brazil	Reference	2.7	4.4	5.7	7.7
	Paris Forever	2.2	3.8	5.0	6.8
	2C-NOW	1.2	2.4	3.4	4.8
	1.5C-NOW	0.8	1.8	2.6	4.0
United States	Reference	-1.7	-4.0	-5.0	-7.5
	Paris Forever	-1.6	-3.6	-4.6	-6.7
	2C-NOW	-1.3	-2.6	-3.2	-3.4
	1.5C-NOW	-1.0	-2.0	-2.4	-2.7
Europe	Reference	-1.2	-2.1	-2.5	-4.3
	Paris Forever	-1.1	-2.0	-2.3	-3.9
	2C-NOW	-1	-1.6	-1.9	-2.8
	1.5C-NOW	-0.8	-1.3	-1.6	-2.3

Table 4. The summary presents the December-February averaged (DJF) results of the relative change in wind power density (units of %). The relative changes reflect the decadal mean differences between the midcentury (2050-2059) from the 2010-2019 average.

Region	Scenario	Area-Average Relative Change in DJF Wind Power Density (%) Calculated Across a Range of Spatial Filters According to Modeled Trend Consensus			
		UF	60%	75%	90%
Globe	Reference	1.7	2.6	4.4	10
	Paris Forever	1.4	2.2	3.8	8.8
	2C-NOW	0.9	1.4	2.5	6.1
	1.5C-NOW	0.6	1.0	1.9	4.6
Central America	Reference	2.0	3.7	6.8	N/A
	Paris Forever	1.7	3.1	6.3	N/A
	2C-NOW	1.0	1.9	4.0	N/A
	1.5C-NOW	0.7	1.3	3.0	N/A
Brazil	Reference	2.9	4.5	6.1	9.4
	Paris Forever	2.5	3.9	5.3	6.4
	2C-NOW	1.5	2.5	3.5	5.2
	1.5C-NOW	1.0	1.9	2.7	1.4
United States	Reference	2.7	4.6	6.0	14.9
	Paris Forever	2.3	3.9	5.2	14.5
	2C-NOW	1.4	2.6	3.6	9.0
	1.5C-NOW	1.0	1.8	2.8	6.9
Europe	Reference	2.8	3.6	4.5	16.8
	Paris Forever	2.4	3.0	3.8	15.4
	2C-NOW	1.5	1.8	2.0	11.2
	1.5C-NOW	1.1	1.3	1.3	6.9

Table 5. The summary presents the March-May averaged (MAM) results of the relative change in wind power density (units of %). The relative changes reflect the decadal mean differences between the midcentury (2050-2059) from the 2010-2019 average.

Region	Scenario	Area-Average Relative Change in MAM Wind Power Density (%) Calculated Across a Range of Spatial Filters According to Modeled Trend Consensus			
		UF	60%	75%	90%
Globe	Reference	1.0	1.5	2.8	8.8
	Paris Forever	0.8	1.2	2.4	7.8
	2C-NOW	0.4	0.6	1.3	4.8
	1.5C-NOW	0.2	0.4	0.9	3.5
Central America	Reference	2.9	4.6	6.2	0.5
	Paris Forever	2.5	4.1	5.6	0.5
	2C-NOW	1.7	2.8	4.0	0.4
	1.5C-NOW	1.3	2.1	3.0	0.4
Brazil	Reference	2.8	4.9	9.2	17.8
	Paris Forever	2.2	4.1	8.2	16.0
	2C-NOW	1.1	2.5	5.4	10.6
	1.5C-NOW	0.6	1.8	4.2	7.8
United States	Reference	-3.2	-5.5	-8.3	-13.7
	Paris Forever	-3.0	-5.0	-7.4	-12.2
	2C-NOW	-2.2	-3.7	-5.3	-8.4
	1.5C-NOW	-1.8	-2.9	-4.1	-6.4
Europe	Reference	0.1	-1.4	-2.0	-15.0
	Paris Forever	-0.1	-1.4	-1.9	-13.4
	2C-NOW	-0.3	-1.3	-1.8	-9.5
	1.5C-NOW	-0.3	-1.1	-1.5	-7.3

Results are presented as area-averaged results for the globe as well as over selected regions: Central America (113W-73W,15N-30N), Brazil (75W-30W, 35S-5N), United States (130W-60W,25N-50N), and Europe (12W-65E,34N-75N). The area-averaged results are shown as a result of varying degrees of model-trend consensus spatial filtering—with grid points excluded from the area-average calculation if they do not exceed the assigned consensus threshold. Also shown are the unfiltered (UF) results. Values of "N/A" indicate insufficient number of grid points that satisfy the consensus criterion to calculate an area-weighted mean.

Table 6. The summary presents the June-August averaged (JJA) results of the relative change in wind power density (units of %). The relative changes reflect the decadal mean differences between the midcentury (2050-2059) from the 2010-2019 average.

Region	Scenario	Area-Average Relative Change in JJA Wind Power Density (%) Calculated Across a Range of Spatial Filters According to Modeled Trend Consensus			
		UF	60%	75%	90%
Globe	Reference	0.3	-0.2	-1.2	-4.2
	Paris Forever	0.1	-0.3	-1.1	-4.0
	2C-NOW	-0.1	-0.4	-1.1	-3.3
	1.5C-NOW	-0.1	-0.4	-0.9	-2.6
Central America	Reference	0.6	0.6	-0.1	11.1
	Paris Forever	0.4	0.4	-0.5	10.1
	2C-NOW	0.0	0.0	-0.4	3.3
	1.5C-NOW	-0.1	-0.1	-0.4	3.2
Brazil	Reference	0.94	1.1	1.5	-10.0
	Paris Forever	0.6	0.8	1.3	-8.6
	2C-NOW	0.0	0.0	0.2	-6.5
	1.5C-NOW	-0.2	-0.1	0.0	-5.1
United States	Reference	-2.2	-4.7	-6.4	-11.1
	Paris Forever	-2.1	-4.2	-5.8	-9.8
	2C-NOW	-1.6	-3.0	-4.1	-6.6
	1.5C-NOW	-1.3	-2.4	-3.2	-4.9
Europe	Reference	-2.1	-3.4	-4.4	-5.7
	Paris Forever	-2.0	-3.1	-4.0	-5.0
	2C-NOW	-1.5	-2.3	-2.9	-4.2
	1.5C-NOW	-1.2	-1.8	-2.3	-3.2

Table 7. The summary presents the September-November averaged (SON) results of the relative change in wind power density (units of %). The relative changes reflect the decadal mean differences between the midcentury (2050-2059) from the 2010-2019 average.

Region	Scenario	Area-Average Median Relative Change in SON Wind Power Density (%) Calculated Across a Range of Spatial Filters According to Modeled Trend Consensus			
		UF	60%	75%	90%
Globe	Reference	1.1	1.5	2.4	3.4
	Paris Forever	0.9	1.2	2.0	2.8
	2C-NOW	0.5	0.7	1.1	1.2
	1.5C-NOW	0.3	0.5	0.8	0.7
Central America	Reference	-2.2	-2.8	-3.0	N/A
	Paris Forever	-2.1	-2.6	-2.7	N/A
	2C-NOW	-1.6	-1.9	-2.0	N/A
	1.5C-NOW	-1.3	-1.5	-1.7	N/A
Brazil	Reference	7.9	9.7	12.6	15.1
	Paris Forever	6.9	8.6	11.1	13.5
	2C-NOW	4.7	5.8	7.5	9.6
	1.5C-NOW	3.5	4.3	5.6	7.4
United States	Reference	-3.5	-6.0	-8.4	-10.2
	Paris Forever	-3.2	-5.5	-7.6	-9.1
	2C-NOW	-2.3	-3.9	-5.3	-6.3
	1.5C-NOW	-1.8	-3.0	-4.1	-4.9
Europe	Reference	-0.6	-1.9	-3.1	-8.2
	Paris Forever	-0.7	-1.8	-2.8	-7.3
	2C-NOW	-0.6	-1.5	-2.3	-5.2
	1.5C-NOW	-0.6	-1.2	-2.0	-3.9

Results are presented as area-averaged results for the globe as well as over selected regions: Central America (113W-73W,15N-30N), Brazil (75W-30W, 35S-5N), United States (130W-60W,25N-50N), and Europe (12W-65E,34N-75N). The area-averaged results are shown as a result of varying degrees of model-trend consensus spatial filtering—with grid points excluded from the area-average calculation if they do not exceed the assigned consensus threshold. Also shown are the unfiltered (UF) results. Values of "N/A" indicate insufficient number of grid points that satisfy the consensus criterion to calculate an area-weighted mean.

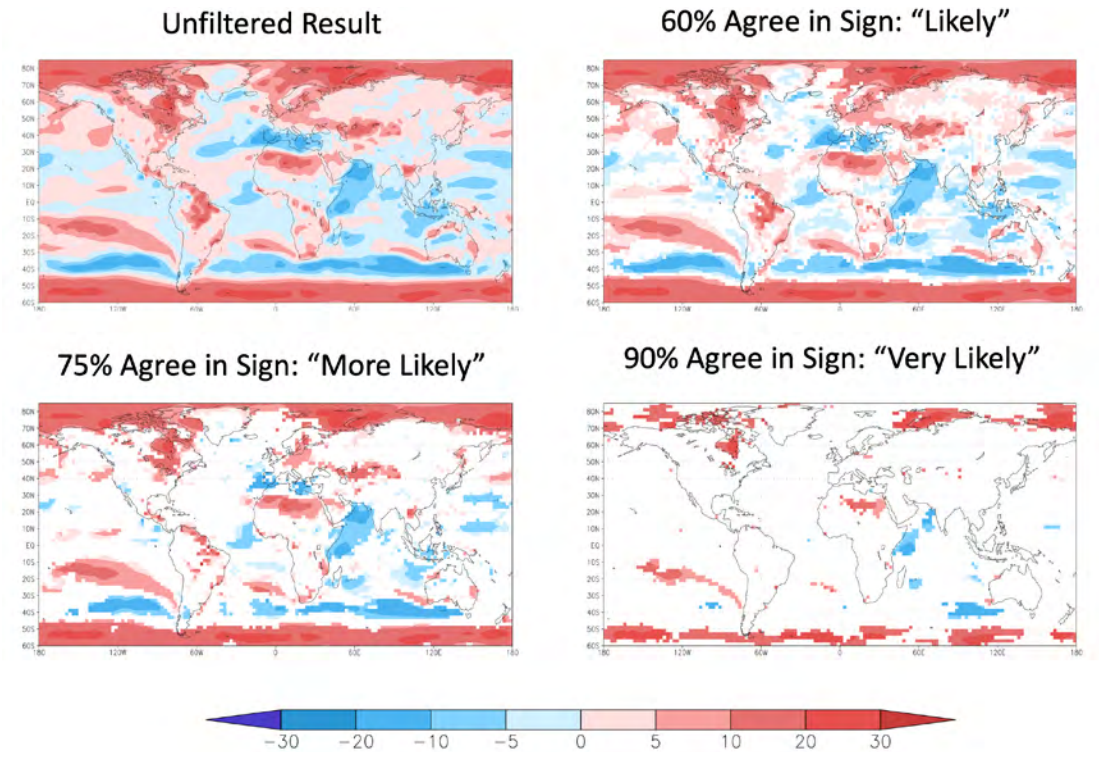

Figure 12. Global results of wind power density (WPD) change by midcentury as simulated in the IGSM Reference scenario. Results shown for the relative change (%) of the decadal averaged Dec-Feb mean WPD for the period 2050-2059 from the 2010-2019 period.

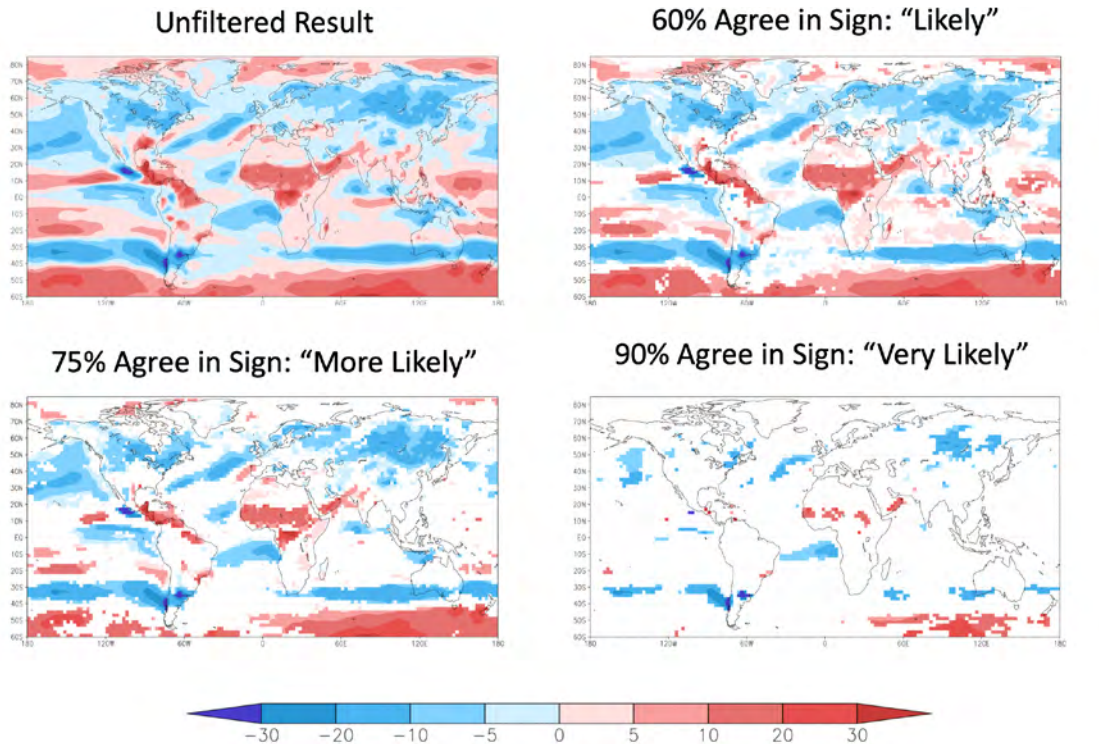

Figure 13. Global results of wind power density (WPD) change by midcentury as simulated in the IGSM Reference scenario. Results shown for the relative change (%) of the decadal averaged Jun-Aug mean WPD for the period 2050-2059 from the 2010-2019 period.

Shaded values represent the mean result from the IGSM ensemble simulation. The upper left panel displays results that have not been filtered, while the remaining panels display the results filtered at the 60% (upper right), 75% (lower left), and 90% (lower right) consensus levels (see text for details).

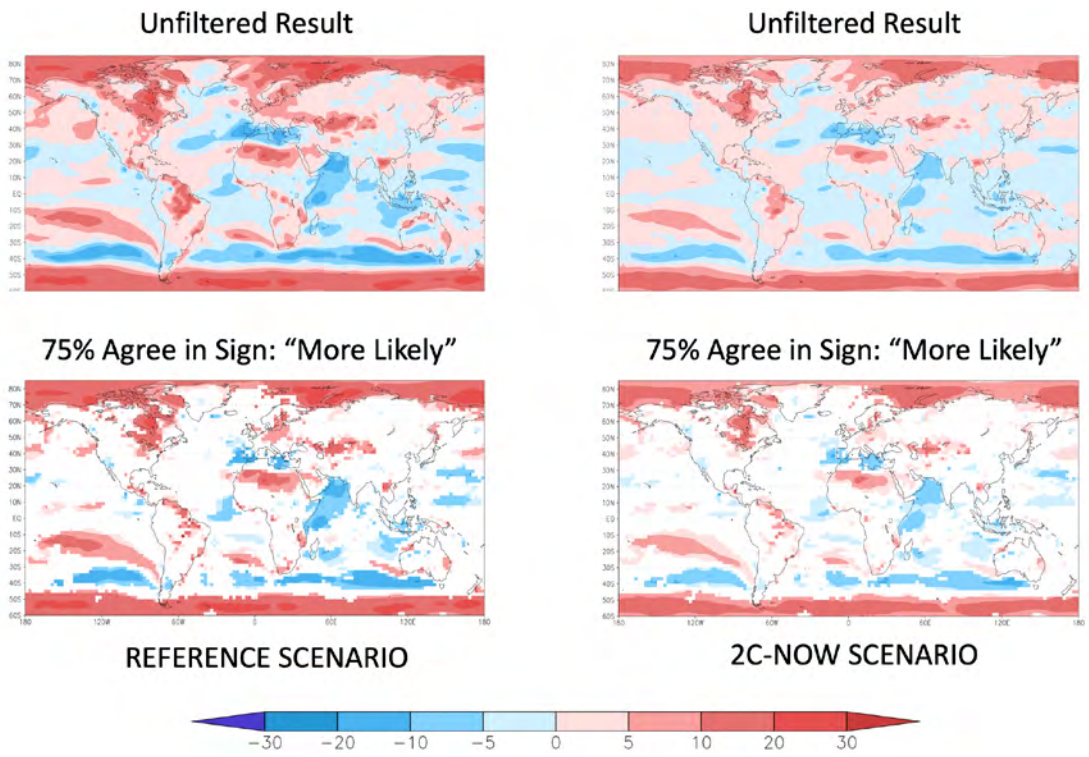

Figure 14. Global results of the IGSM simulated change to wind power density (WPD) by midcentury. Results shown for the relative change (%) of the decadal averaged Dec-Feb mean WPD for the period 2050-2059 from the 2010-2019 period.

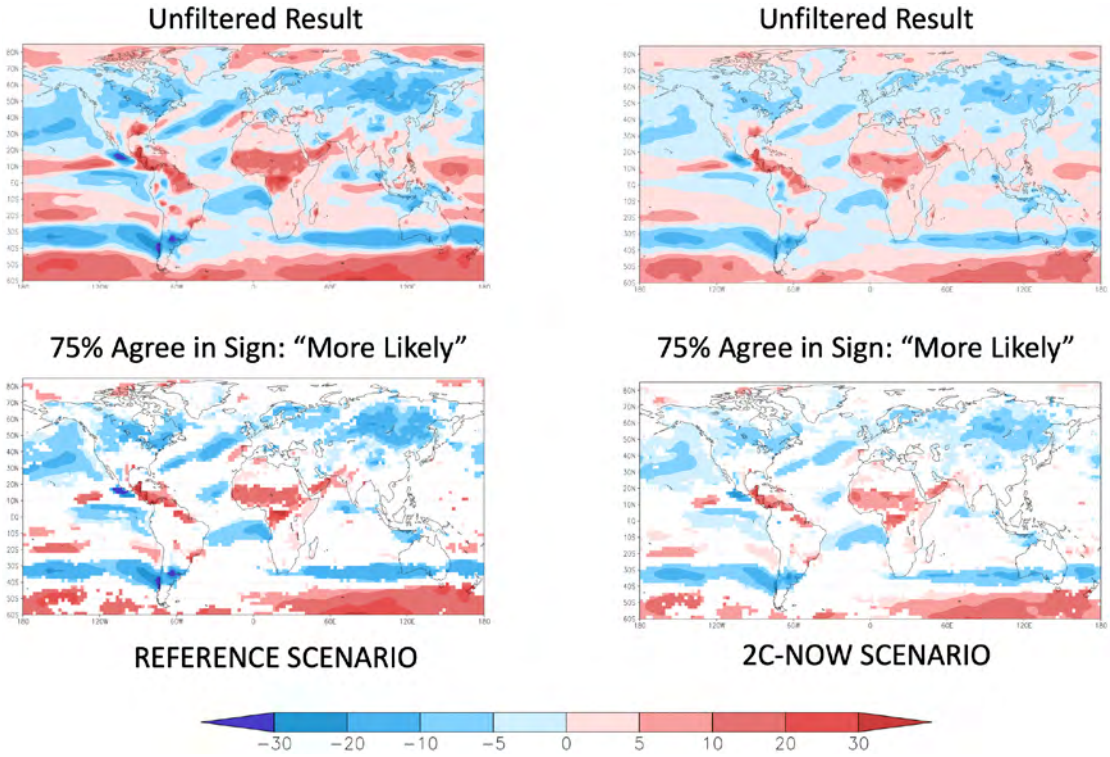

Figure 15. Global results of IGSM-simulated wind power density (WPD) change by midcentury. Results shown for the relative change (%) of the decadal averaged Jun-Aug mean WPD for the period 2050-2059 from the 2010-2019 period.

Shaded values represent the mean result from the IGSM ensemble simulation. The left panels display results from the IGSM Reference scenario, and the right panels display the results from the 2CNOW scenario. The upper panels display results that have not been filtered, while the bottom panels display the results filtered at the 75% consensus level (see text for details).

that are expected across the United States, Europe, and Asia. For these regions, the impact of strong mitigation measures would cut the expected decreases in half over the United States and by one-third over Europe. As previously mentioned, it is important to hightlight, however, that these noted changes would occur only over a fraction of total area of these regions (Table 2). Across most seasons for the regions of interest, the 75% consensus criterion is typically met in 15%-35% of the total area. Nevertheless, the impact of strong mitigation is evident, but the important takeaway is that the moderation of the WPD change—in terms of a beneficial impact or not—indicate a potential for regional trade-offs, which could prove an important factor in global policy and deployment strategies. Further and more detailed investigation is warranted.

3.3 Extreme Quantiles of Change

In light of the ensemble-mean responses, and considering the large ensemble used to construct and determine these responses (across a range of consensus thresholds and scenarios), an additional opportunity to investigate is the potential for low probability of strong changes in WPD. To first order, this was achieved by assessing the asymmetry in the tails of the distribution that were constructed (**Figs. 17 and 18**). In particular, we find that for June-August there is a preponderance of more intense increases than decreases (comparing the 95th percentile to the 5th percentile values) in WPD across tropical lands and the tropical Pacific. Other features to this behavior are consistent with a number of the more salient features of the ensemble mean WPD change: such as a dipole feature across the high latitudes of the southern hemisphere—with a preponderance of more intense decreases across mid-latitudes and more intense increases over high latitudes; more intense decreases than increases over large portions of NH land areas at mid to high latitudes during the summer; and more intense increases across high northern latitudes in winter. Additionally, one feature that is not as clearly distinguishable in the ensemble mean response but more evident under this diagnostic is the notable area of negative skewness across the Atlantic and extending into the Mediterranean region during the NH winter (December-February). This skewness indicates that lowest 5% of the WPD decreases compared to the upper 5% increases may be three times larger in magnitude (upwards of 30-60% decreases compared to upwards of 10% increases). Therefore, this indicates that although each of these regimes in the distribution have equal likelihood of occurring (5% of the total distribution) a potentially "extreme" decrease in WPD is likely to be much stronger than any increase of equal probability. In terms of the ability of strong mitigation to reduce these features, the results indicate that while there is some reduction, even the strongest climate target would not completely remove the risk of these extreme outcomes to occur (**Fig. 18**).

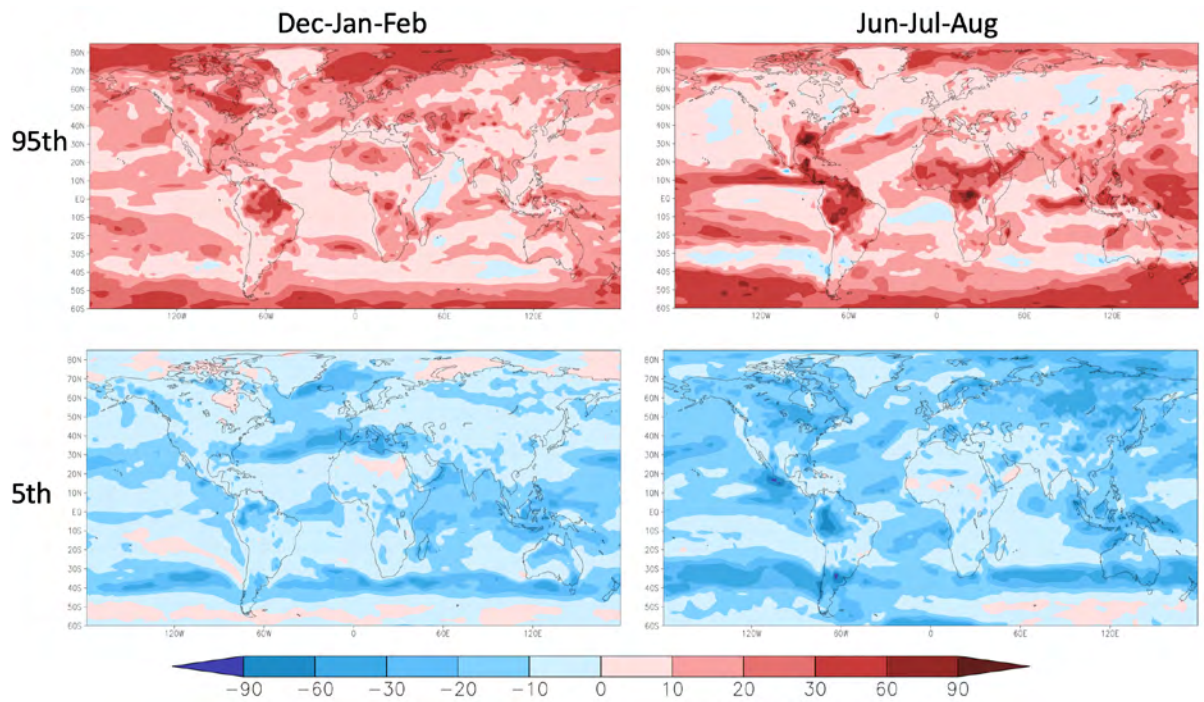

Figure 16. Global results of wind power density (WPD) change by midcentury as simulated in the IGSM Reference scenario. Results are shown for the relative change (%) of the decadal averaged mean WPD for the period 2050-2059 from the 2010-2019 period. In the top panels, shaded values represent the 95th percentile result from the IGSM ensemble simulation, and the bottom panels display the 5th percentile results. The left panels display results averaged for Dec-Feb, and the right panels display the results average for Jun-Aug.

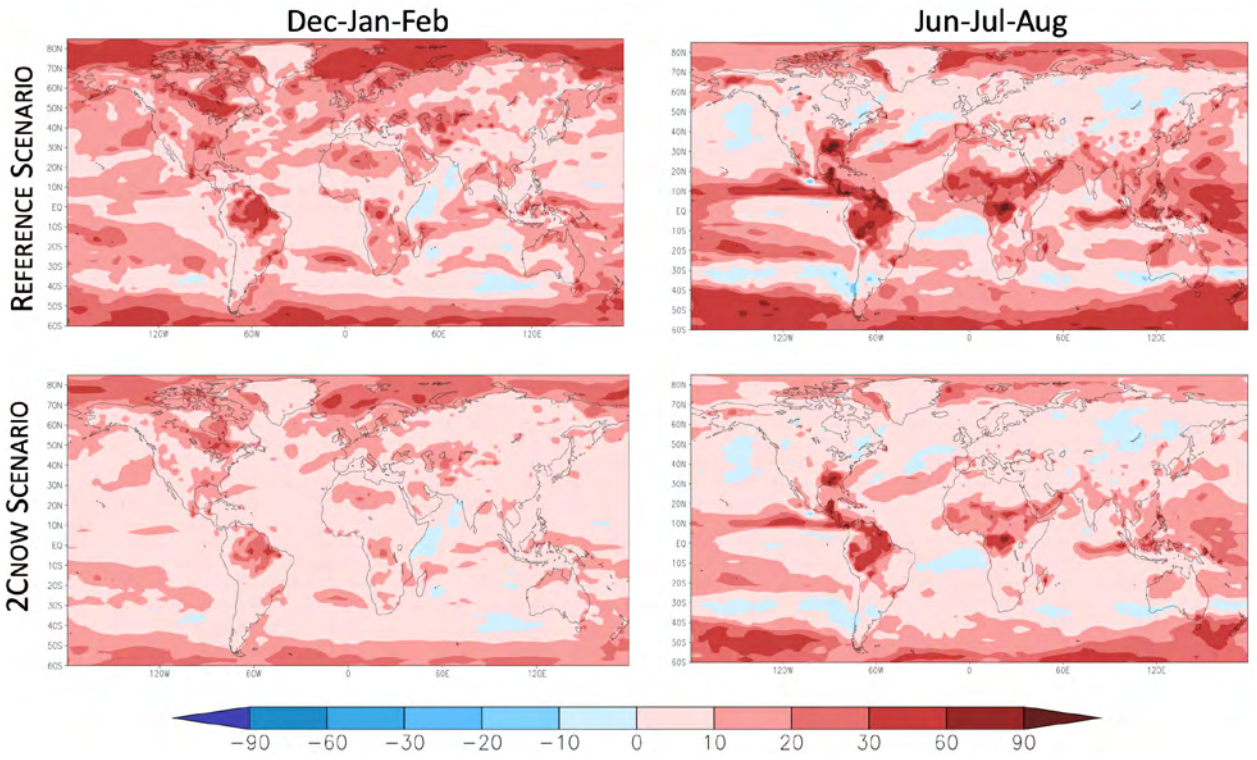

Figure 17. Global results of the IGSM simulated change to wind power density (WPD) by midcentury are displayed. Values shown depict the 95th percentile result from the IGSM simulation. The left panels show results for the relative change (%) of the decadal averaged December-February mean WPD for the period 2050-2059 from the 2010-2019 period, while the right panels display results for June-August. In the top panels, results are given for the IGSM Reference scenario and the bottom panels are from the IGSM 2CNOW scenario.

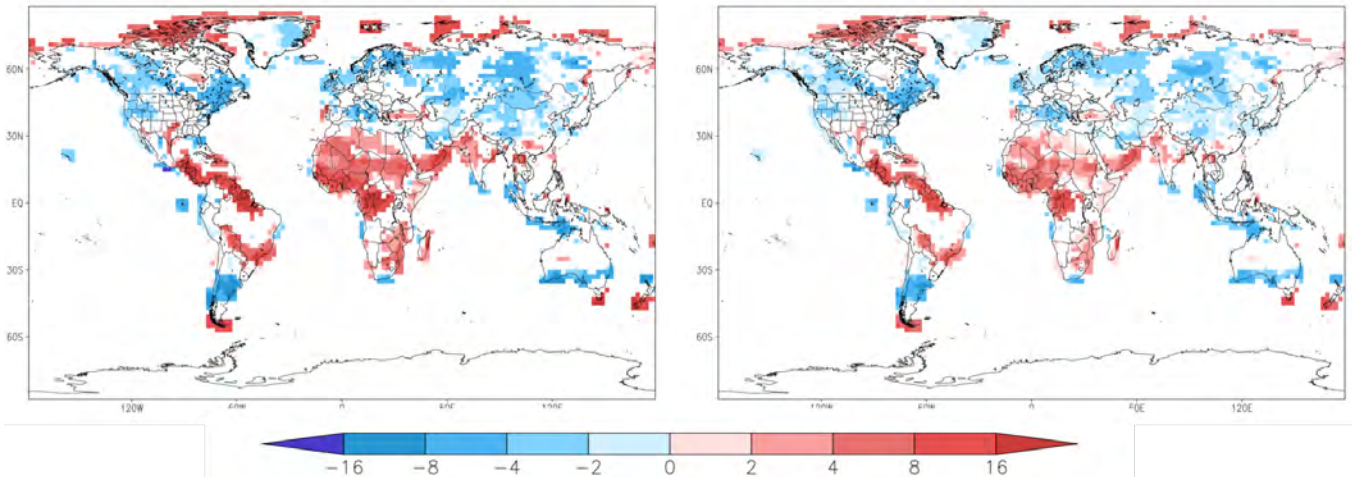

Figure 18. Global results of the change to annual wind power density (WPD) by midcentury as simulated in the IGSM Reference scenario (left panel) and 2CNOW scenario (right panel). Results are shown for the relative change (%) of the decadal averaged mean WPD for the period 2050-2059 from the 2010-2019 period. Shaded values represent the mean result from the IGSM ensemble simulation. In order to highlight potential "offshore" regions of wind power deployment –ocean gridpoints are only shaded if they are in contact with a land grid point (i.e. a "coastal" offshore location). In addition, shaded areas have also been filtered out if the models' consensus in the sign of the trend does not exceed 75%.

3.4 Contrasting Global Onshore and Offshore Wind Power Changes

We further explored the outcomes from these projections under the more practical consideration that any potential deployment of wind farms will largely be contained over land areas as well as near offshore portions of the global ocean. We therefore added additional spatial filtering that isolated grid points that could be considered as either "onshore" and "offshore" regions for wind power deployment. "Onshore" grid points were identified as all land points excluding Antarctica, and all "offshore" grid points were considered as any ocean grid point with at least one its sides in contact with a land point (i.e. a near-coastal ocean area). We then performed similar analyses (Fig. 18 and **Table 8**) as provided in prior sections to assess the global-scale "offshore" and "onshore" wind power consequences under the suite of future climate scenarios.

Among the more salient outcomes of the area-averaged statistics (Table 8), we find that across areas that meet the model-trend consensus threshold, the global, annual wind power density (WPD) will increase slightly offshore (median and average less than 1%) but slightly decrease onshore (-1% in the median). The seasonality of WPD changes is more pronounced, with at least a 75% likelihood that onshore and offshore WPD will increase during December-February and March-May. Conversely, there is a greater chance that an average decrease in WPD will occur during June-August. While the impact of the strong mitigation scenarios is to dampen these changes (reduced by 50-60% from the Reference scenario), the seasonal features to the simulated WPD changes are not removed completely.

In terms of large-scale, coherent patterns of change (Fig. 18), increases in annual WPD are seen across much of the onshore and offshore locations in the tropics, sub-tropics, and high latitudes. In addition, decreased annual WPD dominates much of the extra-tropics (i.e. midlatitudes). There are, however, localized exceptions to both of these characterizations. In particular, at midlatitudes, there are increases seen across a notable portion of southcentral

Table 8. The summary presents the global, annual averaged results of the relative change in wind power density (units of %). The relative changes reflect the decadal mean differences between the midcentury (2050-2059) from the 2010-2019 average. Results are presented as area-averaged results for the global averaged (excluding Antarctica) over onshore (regular font) and offshore (bold font) grid points. For each scenario (Reference, Paris Forever, 2C-NOW, and 15C-NOW), the results for the 25th percentile, median, average (Avg.), and 75th percentile of the ensemble are provided. The area-averaged results are also based on only those points that meet the 66% consensus criterion in the simulated WPD trends. The total percentage area of the offshore and onshore points that meet this criterion is provided in the rightmost column.

	Global Area-Average (excluding Antarctica) Relative Change in Annual Wind Power Density (%)																**% of Area Above Trend Consensus**
	Results for Onshore (top) and **Offshore (bottom)**																Onshore / **Offshore**
	Reference				**Paris Forever**				**2C-NOW**				**15C-NOW**				
	25th	**Med.**	**Avg.**	**75th**	**25th**	**Med.**	**Avg.**	**75th**	**25th**	**Med.**	**Avg.**	**75th**	**25th**	**Med.**	**Avg.**	**75th**	
Annual	-1.6	-1.0	0.0	0.7	-0.5	-0.2	-0.2	0.6	-0.5	-0.2	-0.3	0.2	-0.5	-0.2	-0.3	0.1	49 / **44**
	-0.4	**0.2**	**0.7**	**1.7**	**-0.4**	**0.1**	**0.4**	**1.3**	**-0.5**	**-0.1**	**0.1**	**0.6**	**-0.4**	**-0.2**	**-0.1**	**0.3**	
DJF	1.1	3.2	3.1	4.3	0.9	2.7	2.6	3.7	0.5	1.7	1.7	2.3	0.3	1.2	1.2	1.7	41 / **46**
	1.4	**2.3**	**2.3**	**3.0**	**1.1**	**1.9**	**1.9**	**2.5**	**0.6**	**1.1**	**1.1**	**1.6**	**0.4**	**0.8**	**0.8**	**1.1**	
MAM	0.0	0.6	1.4	2.1	0.0	1.1	1.2	1.8	0.0	0.7	0.7	1.2	-0.1	0.5	0.5	0.9	31 / **29**
	1.8	**2.6**	**2.8**	**3.8**	**1.5**	**2.2**	**2.4**	**3.3**	**0.8**	**1.4**	**1.5**	**2.0**	**0.6**	**1.0**	**1.0**	**1.5**	
JJA	-1.8	-0.9	-1.0	0.3	-1.7	-0.8	-0.9	0.1	-1.2	-0.7	-0.7	0.0	-0.9	-0.5	-0.6	0.0	51 / **34**
	-2.2	**-1.4**	**-0.9**	**0.4**	**-2.0**	**-1.3**	**-0.9**	**0.2**	**-1.5**	**-0.9**	**-0.7**	**0.1**	**-1.2**	**-0.7**	**-0.6**	**0.0**	
SON	-1.1	0.1	-0.2	0.7	-1.0	0.0	-0.3	0.5	-0.8	-0.1	-0.3	0.3	-0.7	-0.1	-0.2	0.2	41 / **41**
	0.3	**1.3**	**1.1**	**2.5**	**0.2**	**1.0**	**0.9**	**2.1**	**0.0**	**0.5**	**0.4**	**1.2**	**0.0**	**0.3**	**0.2**	**0.8**	

United States and just offshore of Portugal and Spain. In addition, a number of offshore locations across the tropics experience a decrease in WPD that contrasts increased WPD in neighboring onshore areas. These offshore areas are found along western Africa, Brazil, Peru, Ecuador, and southern India. The global patterns of WPD change are largely preserved in the 2°C climate-target scenario, but consistent with the area-averaged results the magnitudes of the changes are diminished.

4. Closing Remarks

We have employed a hybrid method that combines the emerging patterns of change in near-surface winds from the CMIP5 model collection with the large-ensemble, probabilistic projections of the MIT IGSM. This procedure has provided a comprehensive set of outcomes to explore the potential for changing WPD patterns under a range of human-forced climate trajectories. Our key results can be summarized as follows:

- Globally speaking, at a "75% consensus" threshold criterion (at least 3 out of every 4 members agree in sign), by mid-century under the Reference scenario an increase of about 2% in annual-averaged WPD is expected. Under the most aggressive mitigation scenario considered, 15CNOW, the expected increase is reduced to 0.5%.
- There is a notable seasonality to the expected global changes. During the December-February period, globally and across all regions of interest, the ensemble-mean response (at the %75 consensus) indicates increases in WPD to expected by mid-century even under the strongest mitigation actions. Decreases in ensemble-mean WPD by midcentury even under the strongest mitigation measures are expected over the United States and Europe during Spring, Summer, and Fall. These decreases are on the order of -6% to -3% of current conditions.
- Tightening the consensus criterion substantially reduces the total area of the globe for which these WPD changes can be considered. At 90% consensus (at least 9 out of every 10 ensemble members must agree in sign of change) only 5%-8% of globe passes this threshold in the ensemble of WPD changes. Nevertheless, in these isolated areas of "high consensus" regions (90% consensus) decreases in onshore WPD are expected by midcentury over portions of mid-to-high latitude land areas during the Northern Hemisphere summer months. Conversely, increases are seen across northern Africa.
- For the regionally averaged domains considered in this study at the 75% consensus level, annual averaged WPD is expected to increase over Brazil, and decrease over Central America, (continental) United States, and Europe. This also occurs for seasonally averages changes during the JJA and SON periods. In particular, by mid-century the largest relative increase in annual WPD change is seen over Brazil (this area average includes the Amazon region) at 5.7%, and the largest decrease occurs over the (continental) United States at –5%, as a result from the Refence scenario. During DJF—the regionally averaged WPD for all area-averaged domains considered is expected to increase by midcentury. This occurs for all the scenarios considered. Under the Paris Forever scenario, the range of relative area-averaged WPD changes is 3.8 – 6.3% for the regions considered.
- Across areas that meet the consensus threshold in the direction of change—global, annual wind power density (WPD) will increase slightly offshore (median and average less than 1%) but slightly decrease onshore (-1% in the median). The seasonality of WPD changes is more pronounced, with onshore and offshore increases during DJF and MAM periods and decreases during JJA. Increases in annual WPD are seen across much of the onshore/offshore tropics, sub-tropics, and high latitudes. Decreased annual WPD dominates much of the extra-tropics (i.e. midlatitudes) with some localized exceptions. The global patterns of WPD change are largely preserved in the 2°C climate-target scenario.

In light of all these interpretations—it is important to recognize that WPD is a metric that describes the cross-sectional unit-area (with respect to the turbine blade) change of wind power resource. Therefore, when considering how the wind power industry can cope, adapt, and in some cases, take advantage of the anticipated changes—the wind power industry can use the WPD information from this study to set long-term, large-scale strategic deployment of: larger turbine blades, turbine height (i.e. higher height results in typically stronger windspeeds) and more efficient generation technologies.

A number of aspects in this research warrant and merit further investigation. When considering the landscape of WPD changes depicted under the 75%-consensus criterion, there are large-scale features to the ensemble-mean patterns that may have a physical explanation. In doing so, this would also offer further credibility as to whether these indicated changes are an expression of inherent predictability of the climate system to human-forced change—and whether to act upon these anticipated changes. The widespread decreases in WPD across the NH land regions during the warmer seasons, but with increases expected during the winter, may pose considerable technical and deployment challenges to long-term storage technologies, which include not only turbine technology but large-scale storage technologies and deployment.

This study considered the changes in ***mean*** annual and seasonal wind power resource and was not able to consider the changes in daily and sub-daily intermittency. This was due, in large part, to the unavailability of the CMIP5

model outputs of near-surface windspeed at daily and hourly timescales. However, the completion of the CMIP Phase 6 simulations and their availability to the research community can allow for the same pattern-change kernel responses to be assessed. In this way, a more comprehensive examination and quantification of risk to the future availability and intermittency of wind power resources would be achievable.

To further the ability to provide a more detailed examination of the regional and local aspects of wind power resources, more extensive experimentation and examination with regional climate models (RCMs) is also warranted. However, such an exercise that would provide the commensurate rigor to the CMIP model collection would come at a considerable computational extent and cost. The international climate model community has undertaken a number of coordinated experiments (e.g. CORDEX), and therefore comparative examinations are possible. Yet, more extensive examinations and further coordinated numerical experiments would prove valuable in this regard.

In view of all these considerations, several follow-up studies would be of considerable interest. For example, a study that incorporates the most up-to-date results of global climate models (i.e. the models from CMIP6 are more than double that of CMIP5 used in this study) in conjunction with CORDEX and other supporting results from regional climate models. Combined, this pool of model simulations would provide a deeper insight not only to the mean shifts in WPD, but also assess expected global changes in wind power availability and intermittency. An additional companion study of interest could also assess changes in solar power, using similar historical and future climate/weather information. In tandem with a wind power assessment, these can also assess the co-evolving nature of changing risk to renewable resources and intermittency under anticipated human-forced, climate-related change. Further, modeling tools exist in the scientific community that allow for a more detailed and process-oriented investigation of the localized and/or downstream effects of widespread wind-farm installations. Such models could be exercised over regions/areas noted in this assessment with elevated risk of change that are important strategically for long-term development and site-specific deployment.

Acknowledgments

The authors gratefully acknowledge support from Iberdrola for this study. In addition, general financial support for the MIT Joint Program on the Science and Policy of Global Change is provided through a consortium of industrial sponsors and Federal grants. The authors also wish to thank International Mentoring Foundation for the Advancement of Higher Education fellowship in support of Sara Uzquiano Perez's research internship that contributed to this study. Development of the IGSM applied in this research was supported by the U.S. Department of Energy, Office of Science (DE-FG02-94ER61937); the U.S. Environmental Protection Agency, EPRI, and other U.S. government agencies and a consortium of 40 industrial and foundation sponsors. For a complete list see https://globalchange.mit.edu/sponsors/current.

5. References

Chen, Y.-H.H., S. Paltsev, J.M. Reilly, J.F. Morris and M.H. Babiker (2016). Long-term economic modeling for climate change assessment. *Economic Modelling*, 52(Part B): 867–883. (http://www.sciencedirect.com/science/article/pii/S0264999315003193)

Cosseron, A., U.B. Gunturu, and C.A. Schlosser (2013). Characterization of the Wind Power Resource in Europe and its Intermittency, *Energy Procedia,* 40, 58-66, http://dx.doi.org/10.1016/j.egypro.2013.08.008

De Castro, C., Mediavilla, M., Miguel, L.J., Frechoso, F., 2011. Global wind power potential: physical and technological limits. Energy Policy 39 (10), 6677–6682.

Gao, Y., S. Ma, and T. Wang (2019). The impact of climate change on wind power abundance and variability in China, *Energy*, **189**, https://doi.org/10.1016/j.energy.2019.116215.

Enevoldsena, P., F.-H. Permienb, I. Bakhtaouic, A.-K. von Kraulande, M.Z. Jacobson, G. Xydis, B.K. Sovacool, S.V. Valentine, D. Luecht, G. Oxley (2019). How much wind power potential does Europe have? Examining European wind power potential with an enhanced socio-technical atlas. *Energy Policy*, 132, 1092–1100, https://doi.org/10.1016/j.enpol.2019.06.064.

Eurek, K., P. Sullivan, M. Gleason, D. Hettinger, D. Heimiller, and A. Lopez (2017). An improved global wind resource estimate for integrated assessment models, *Energy Economics*, **64**, 552–567.

Fant, C., Gunturu U.B., and C.A. Schlosser (2016). Characterizing wind power resource reliability in southern Africa, *Applied Energy,* **161**, 565-573, ISSN 0306-2619, http://dx.doi.org/10.1016/j.apenergy.2015.08.069.

Frieler, K., M. Meinshausen, M. Mengel, N. Braun, and W. Hare (2012). A scaling approach to probabilistic assessment of regional climate change, *J. Clim.*, 25(9), 3117–3144, doi:10.1175/JCLI-D-11-00199.1.

Gunturu, U.B and C.A. Schlosser (2012): Characterization of wind power resource in the United States. *Atmospheric Chemistry and Physics*, 12: 9687-9702(http://dx.doi.org/10.5194/acp-12-9687-2012)

Hallgren, W., U.B. Gunturu and A. Schlosser (2014). The Potential Wind Power Resource in Australia: A New Perspective, PLoS ONE, 9(7): e99608, doi: 10.1371/journal.pone.0099608

Herger, N., B.M. Sanderson, and R. Knutti (2015). Improved pattern scaling approaches for the use in climate impact studies, Geophys. Res. Lett., 42, doi:10.1002/2015GL063569.

Jung, C., and D. Schindler (2019). Changing wind speed distributions under future global climate, *Energy Conversion and Management*. https://doi.org/10.1016/j.enconman.2019.111841.

Jung, C., D. Taubert, and D. Schindler (2019). The temporal variability of global wind energy – long-term trends and inter-annual variability, *Energy Conversion and Management*, **188**, 462-472.

Karnauskas, K., J.K. Lundquist, and L. Zhang (2017). Southward shift to the global wind energy resource under high carbon dioxide emissions, *Nature Geosci.*, https://doi.org/10.1038/s41561-017-0029-9.

Kriesche, P. and C.A. Schlosser (2014). The Association of the North Atlantic and the Arctic Oscillation on Wind Energy Resource over Europe and its Intermittency, *Energy Procedia,* 59, 270-277.

Lee, J.C.Y., M.J. Fields, and J.K. Lundquist (2018). Assessing variability of wind speed: comparison and validation of 27 methodologies, Wind Energ. Sci., 3, 845–868, https://doi.org/10.5194/wes-3-845-2018

Libardoni, A.G., C.E. Forest, A.P. Sokolov and E. Monier (2018): Estimates of climate system properties incorporating recent climate change. *Advances in Statistical Climatology, Meteorology and Oceanography*, 4(1/2),19-36 (doi:10.5194/ascmo-4-19-2018) (https://www.adv-stat-clim-meteorol-oceanogr.net/4/19/2018/)

Liu, F., F. Sun, W. Liu, T. Wang, H. Wang, X. Wang, W.H. Lim (2019). On wind speed pattern and energy potential in China, *Applied Energy*, **236**, 867-876, https://doi.org/10.1016/j.apenergy.2018.12.056.

Lopez, A., E.B. Suckling, and L.A. Smith (2013). Robustness of pattern scaled climate change scenarios for adaptation decision support, Clim. Change, 122(4), 555–566, doi:10.1007/s10584-013-1022-y.
Luderer, G., R.C. Pietzcker, S. Carrara, H. Sytze de Boer, S. Fujumori, N. Johnson, S. Mima, and D. Arent (2017). Assessment of wind and solar power in global low-carbon energy scenarios: An introduction, *Energy Economics*, **64,** 542-551.

Mitchell, T.D. (2003). Pattern scaling—An examination of the accuracy of the technique for describing future climates, Clim. Change, 60(3), 217 – 242.

Reifen, C., and R. Toumi, 2009, Climate projections: Past performance no guarantee of future skill?, *Geophys. Res. Lett.*, **36**, doi:10.1029/2009GL038082.

Reilly, J., Y-H Chen, Y-H., A. Sokolov, X. Gao, A. Schlosser, J. Morris, E. Monier, S. Paltsev, 2018. Food, Water, Energy, Climate Outlook, 2018, MIT Joint Program on the Science and Policy of Global Change, https://globalchange.mit.edu/outlook2018.

Rienecker, M.M., Suarez, M.J., Gelaro, R., Todling, R., Bacmeister, J., Liu, E., Bosilovich, M.G., Schubert, S.D., Takacs, L., Kim, G.-K., Bloom, S., Chen, J., Collins, D., Conaty, A., da Silva, A., Gu, W., Joiner, J., Koster, R.D., Lucchesi, R., Molod, A., Owens, T., Pawson, S., Pegion, P., Redder, C.R., Reichle, R., Robertson, F.R., Ruddick, A.G., Sienkiewicz,M., and Woollen, J., 2011. MERRA: NASAs modern-era retrospective analysis for research and applications". *J. Climate*, 24(14), July, pp. 3624-3648.

Santer, B.D., T.M.L. Wigley, M.E. Schlesinger, and J.F.B. Mitchell (1990). Developing climate scenarios from equilibrium GCM results, *Tech. Rep.*, Max–Planck-Institut für Meteorologie, Hamburg, Germany.

Schlosser, C.A., X. Gao, K. Strzepek, A. Sokolov, C.E. Forest, S. Awadalla, W. Farmer (2012): Quantifying the Likelihood of Regional Climate Change: A Hybridized Approach. *Journal of Climate*, 26(10): 3394-3414 (http://dx.doi.org/10.1175/JCLI-D-11-00730.1)

Sokolov, A., Kicklighter, D., Schlosser, A., Wang, C., Monier, E., Brown-Steiner, B., *et al.* (2018). Description and Evaluation of the MIT Earth System Model (MESM). Journal of Advances in Modeling Earth Systems, 10, 1759–1789. https://doi.org/10.1002/2018MS001277

Taylor, K.E., R.J. Stouffer, G.A. Meehl (2012). An Overview of CMIP5 and the experiment design. Bull. Amer. Meteor. Soc., **93**, 485-498, doi:10.1175/BAMS-D-11-00094.1.

Tian, Q., G. Huang, K. Hu, and D. Niyogi (2018). Observed and global climate model based changes in wind power potential over the Northern Hemisphere during 1979-2016, *Energy*, **167**, https://doi.org/10.1016/j.energy.2018.11.027.

Torralba, V., F.J. Doblas-Reyes, and N. Gonzalez-Revireigo (2017). Uncertainty in recent near-surface wind speed trends: a global reanalysis intercomparison, *Environ. Res. Lett*, https://doi.org/10.1088/1748-9326/aa8a58.

Ulazia, A., J. Saenz, G. Ibarra-Berastegi, S.J. Gonzalez-Rojí, and S. Carreno-Madinabeitia (2019). Global estimations of wind energy potential considering seasonal air density changes, *Energy*, https://doi.org/10.1016/j.energy.2019.115938.

Wang, C., and R.G. Prinn, 2010: Potential climatic impacts and reliability of very large-scale wind farms. *Atmos. Chem. Phys.*, **10**, 2053–2061, doi:10.5194/acp-10-2053-2010.

Wigley, T.M.L., Raper, S.C.B., Smith, S., and Hulme, M.: 2000, *The MAGICC/SCENGEN Climate Scenario Generator: Version 2.4: Technical Manual*, CRU, UEA, Norwich, U.K.

Zeng, Z., A.D. Ziegler, T. Seachinger, L. Yang, A. Chen, K. Ju, S. Piao, L.Z.X. Li, P. Ciasis, D. Chen. J. Liu, C. Azorin-Molina, A. Chappell, D. Medvigy, and E.F. Wood (2019). A reversal in global terrestrial stilling and its implications for wind energy production, *Nature Climate Change*, **9,** 979-985, https://doi.org/10.1038/s41558-019-0622-6.

Joint Program Report Series - Recent Articles

For limited quantities, Joint Program Reports are available free of charge. Contact the Joint Program Office to order.
Complete list: http://globalchange.mit.edu/publications

357. **The Changing Nature of Climate-Related Risks in Global Wind Power Resources.** *Schlosser et al., Dec 2021*

356. **Transition Scenarios for Analyzing Climate-Related Financial Risk.** *Chen et al., Jan 2022*

355. **Economic Analysis of the Hard-to-Abate Sectors in India.** *Paltsev et al., Sep 2021*

354. **Distributional Impacts of Low-Carbon Policies in USA and Spain: Does One Size Fit All?** *Garcia-Muros et al., Aug 2021*

353. **Predictability of U.S. Regional Extreme Precipitation Occurrence Based on Large-Scale Meteorological Patterns (LSMPs).** *Gao & Mathur, Jun 2021*

352. **Toward Resilient Energy Infrastructure: Understanding the Effects of Changes in the Climate Mean and Extreme Events in the Northeastern United States.** *Komurcu & Paltsev, Jun 2021*

351. **Meeting Potential New U.S. Climate Goals.** *Yuan et al., Apr 2021*

350. **Hydroclimatic Analysis of Climate Change Risks to Global Corporate Assets in Support of Deep-Dive Valuation.** *Strzepek et al., Apr 2021*

349. **A Consistent Framework for Uncertainty in Coupled Human-Earth System Models.** *Morris et al., Mar 2021*

348. **Changing the Global Energy System: Temperature Implications of the Different Storylines in the 2021 Shell Energy Transformation Scenarios.** *Paltsev et al., Feb 2021*

347. **Representing Socio-Economic Uncertainty in Human System Models.** *Morris et al., Feb 2021*

346. **Renewable energy transition in the Turkish power sector: A techno-economic analysis with a high-resolution power expansion model, TR-Power.** *Kat, Feb 2021*

345. **The economics of bioenergy with carbon capture and storage (BECCS) deployment in a 1.5°C or 2°C world.** *Fajardy et al., Nov 2020*

344. **Future energy: In search of a scenario reflecting current and future pressures and trends.** *Morris et al., Nov 2020*

343. **Challenges in Simulating Economic Effects of Climate Change on Global Agricultural Markets.** *Reilly et al., Aug 2020*

342. **The Changing Nature of Hydroclimatic Risks across South Africa.** *Schlosser et al., Aug 2020*

341. **Emulation of Community Land Model Version 5 (CLM5) to Quantify Sensitivity of Soil Moisture to Uncertain Parameters.** *Gao et al., Feb 2020*

340. **Can a growing world be fed when the climate is changing?** *Dietz and Lanz, Feb 2020*

339. **MIT Scenarios for Assessing Climate-Related Financial Risk.** *Landry et al., Dec 2019*

338. **Deep Decarbonization of the U.S. Electricity Sector: Is There a Role for Nuclear Power?** *Tapia-Ahumada et al., Sep 2019*

337. **Health Co-Benefits of Sub-National Renewable Energy Policy in the U.S.** *Dimanchev et al., Jun 2019*

336. **Did the shale gas boom reduce US CO_2 emissions?** *Chen et al., Apr 2019*

335. **Designing Successful Greenhouse Gas Emission Reduction Policies: A Primer for Policymakers – The Perfect or the Good?** *Phillips & Reilly, Feb 2019*

334. **Implications of Updating the Input-output Database of a Computable General Equilibrium Model on Emissions Mitigation Policy Analyses.** *Hong et al., Feb 2019*

333. **Statistical Emulators of Irrigated Crop Yields and Irrigation Water Requirements.** *Blanc, Aug 2018*

332. **Turkish Energy Sector Development and the Paris Agreement Goals: A CGE Model Assessment.** *Kat et al., Jul 2018*

331. **The economic and emissions benefits of engineered wood products in a low-carbon future.** *Winchester & Reilly, Jun 2018*

330. **Meeting the Goals of the Paris Agreement: Temperature Implications of the Shell Sky Scenario.** *Paltsev et al., Mar 2018*

329. **Next Steps in Tax Reform.** *Jacoby et al., Mar 2018*

328. **The Economic, Energy, and Emissions Impacts of Climate Policy in South Korea.** *Winchester & Reilly, Mar 2018*

327. **Evaluating India's climate targets: the implications of economy-wide and sector specific policies.** *Singh et al., Mar 2018*

326. **MIT Climate Resilience Planning: Flood Vulnerability Study.** *Strzepek et al., Mar 2018*

325. **Description and Evaluation of the MIT Earth System Model (MESM).** *Sokolov et al., Feb 2018*

324. **Finding Itself in the Post-Paris World: Russia in the New Global Energy Landscape.** *Makarov et al., Dec 2017*

323. **The Economic Projection and Policy Analysis Model for Taiwan: A Global Computable General Equilibrium Analysis.** *Chai et al., Nov 2017*

MIT Joint Program on the Science and Policy of Global Change

Massachusetts Institute of Technology
77 Massachusetts Ave., E19-411
Cambridge MA 02139-4307 (USA)

T (617) 253-7492 **F** (617) 253-9845
globalchange@mit.edu
http://globalchange.mit.edu/